



Phase Equilibria in the Ti-Rich Part of the Ti-Al-Nb System— Part I: Low-Temperature Phase Equilibria Between 700 and 900 °C

B. Distl¹ · K. Hauschildt² · B. Rashkova³ · F. Pyczak² · F. Stein¹

Submitted: 14 March 2022 / in revised form: 26 April 2022 / Accepted: 18 May 2022 / Published online: 1 July 2022
© The Author(s) 2022

Abstract Precise knowledge of the phase equilibria in the Ti-Al-Nb system between 700 and 900 °C is of crucial importance for the urgently needed improvement of TiAl-based turbine materials already in industrial use to achieve further energy savings. As a result of the occurrence of the two ternary intermetallic phases ω_0 (“Ti₄NbAl₃”) and O (“Ti₂NbAl”), which form in the solid state just in the range of the application-relevant temperatures, the phase relations are very complex and not well studied. In the present investigation, isothermal sections of the Ti-rich part of the Ti-Al-Nb system at 700, 800, and 900 °C were determined by a systematic study of 15 ternary alloys, one solid-solid diffusion couple, and three liquid-solid diffusion couples. Using scanning electron microscopy, electron probe microanalysis (EPMA), x-ray diffraction (XRD), high-energy XRD (HEXRD), differential thermal analysis (DTA), and transmission electron microscopy (TEM) investigations, type and composition of phases as well as phase transitions were determined. With these results, the phase equilibria were established. A focus of the investigations is on the homogeneity ranges of the two ternary phases ω_0 and O, which both are stable up to temperatures above 900 °C. Based on the compositions measured for the ω_0 phase and its crystal structure type, a new formula (Ti,Nb)₂Al is suggested. The results also indicate that the

phase field of the ω_0 phase is split into two parts at 900 °C because of the growing phase field of the ordered (β Ti,Nb)₀ phase.

Keywords diffusion couples · experimental phase equilibria · intermetallics · isothermal section · phase diagram

1 Introduction

In the ongoing efforts to reduce CO₂ and NO_x emissions from turbine jet engines, the Ti-Al-rich phase equilibria of the Ti-Al-Nb system between 700 and 900 °C play a crucial role. This is due to the facts that: (i) titanium aluminides in general show a very promising light-weight design potential compared to the currently used Ni-based superalloys due to their high specific strength;^[1,2] (ii) currently used TiAl-based alloys, such as 4822 (Ti-48Al-2Nb-2Cr)^[3] and TNM (Ti-43.5Al-4Nb-1Mo-0.1B)^[4] (here and in the following, all alloy compositions are given in at.%), rely on the addition of elements such as Nb to achieve the mechanical properties required for their use as high-temperature structural materials;^[2,3] (iii) 700 to 900 °C is the desired application temperature range for next generation turbine blades.^[5,6] The occurring phases and their phase equilibria play a crucial role in optimizing the microstructure, which is a key factor for obtaining improved mechanical properties.^[1,4,5]

Besides the disordered solid solution phases (α Ti) and (β Ti,Nb) (which can exhibit B2-ordering by addition of alloying elements^[7]) and the binary intermetallic phases Ti₃Al (also designated as α_2 phase), TiAl (also designated as γ phase), Nb₂Al, and Nb₃Al, two ternary intermetallic

✉ B. Distl
distl@mpie.de

✉ F. Stein
stein@mpie.de

¹ Max-Planck-Institut für Eisenforschung GmbH, Düsseldorf, Germany

² Helmholtz Zentrum Hereon, Geesthacht, Germany

³ Montanuniversität Leoben, Leoben, Austria

phases, the so-called ω_o (“Ti₄NbAl₃”) and O (“Ti₂NbAl”) phase, are present in alloys in the Ti-rich part of the system. The crystallographic information of the mentioned phases is summarized in Table 1. Literature data indicate that both ternary phases exhibit an extended, but not yet well-defined homogeneity range at temperatures up to 900 °C. They are thermodynamically unstable at high temperatures and decompose in solid state reactions above 900 °C.^[8] In particular the O phase has attracted a lot of attention in recent years. Alloys based on this phase were found to have improved room-temperature ductility and fracture toughness compared to the above mentioned TiAl-based alloys.^[9]

For further alloy development, a detailed knowledge of the phase equilibria over the entire composition range between 0–50 at.% Al and 0–30 at.% Nb is mandatory. However, especially for the application-relevant temperature range between 700 and 900 °C, the available information from literature is very limited and no systematic experimental study of phase relations in this composition and temperature range has been performed.

Experimental work on (in most cases partial) isothermal sections in this temperature range was reported in Refs. [17–22]. Pavlov et al.^[17] studied phase equilibria in a series of Nb-rich alloys heat-treated at 900 °C. Their results are limited exclusively to the Nb-rich corner of the system (< 40 at.% Ti). Rowe et al.^[18] were interested in the solubility of Al in the (β Ti,Nb) solid solution and its phase relations to the O phase at 900 °C. They established a partial isothermal section in the range between 5–25 at.% Al and 10–40 at.% Nb showing the equilibria between the O phase, (β Ti,Nb), and Ti₃Al including the three-phase equilibrium. Miracle et al.^[19] studied some alloys in the same composition range (fixed Al content of 22 at.% Al), but their data did not allow to determine the O phase + (β Ti,Nb) + Ti₃Al triangle. In his doctoral thesis, Sadi^[20] performed experimental investigations on phase equilibria

in the temperature range 700–900 °C using seven Ti–Al–Nb alloys in the composition range of the O and ω_o phase. Even though he determined various tie-triangles and tie-lines, his data are partially inconsistent. In his thesis and in later publications,^[21,23] he presented isothermal sections which relied on calculations based on the thermodynamic database of Servant and Ansara^[24] and not on his own experimental data. The only complete isothermal section in the investigated temperature range based on experimental work was presented recently by Xu et al.^[22] for 900 °C. They derived local phase equilibria from extrapolations to phase interfaces obtained in a diffusion multiple consisting of Ti, Nb, Ti-73Al, Ti-40Nb, and Ti-60Nb annealed at 900 °C for 6000 h. No experimental sections for 700 and 800 °C were reported in the literature.

Some information on equilibria at these temperatures is available from vertical sections reported in the literature, but almost all of them are limited to the range of the O phase along constant Al contents of 22 at.%,^[19,25–27] 25 at.%,^[28–30] and 27.5 at.%.^[31] Only exceptions are a vertical section along 50 at.% Ti from Bendersky et al.^[32] and a section along 8 at.% Nb presented by Xu et al.^[33] However, in case of the 50 at.% Ti section, this is only an estimated schematic based on two alloys.^[32] In case of the 8 at.% Nb section, the authors mention that “because of the actual preparation process, the experimental isopleth showed metastable phase behavior”.^[33]

Based on the experimental data available at the time, isothermal sections were also obtained using thermodynamic modelling. In 1992, Kattner and Boettinger^[34] presented a rough isothermal section at 700 °C. Their thermodynamic description was slightly updated some years later by Servant and Ansara^[24] and finally another updated description was reported in 2009 by Witusiewicz et al.^[35] However, the calculated sections at 700 to 900 °C still cannot describe the experimental data very well, as was also recently noted by Xu et al.^[22] A major reason for

Table 1 Phases and their crystal structures occurring in phase equilibria in the Ti-rich part of the Ti–Al–Nb system between 700 and 900 °C

Phase	Crystal system	Pearson symbol	Space group	Strukturbericht designation	Reference
(α Ti)	Hexagonal	<i>hP2</i>	<i>P6₃/mmc</i>	A3	[10]
(β Ti,Nb)	Cubic	<i>cI2</i>	<i>Im-3m</i>	A2	[10]
(β Ti,Nb) _o	Cubic	<i>cP2</i>	<i>Pm-3m</i>	B2	[10]
Ti ₃ Al, α_2	Hexagonal	<i>hP8</i>	<i>P6₃/mmc</i>	D0 ₁₉	[11]
TiAl, γ	Tetragonal	<i>tP4</i>	<i>PA/mmm</i>	L1 ₀	[12]
Nb ₂ Al	Tetragonal	<i>tP30</i>	<i>PA₂/mnm</i>	D8 _b	[13]
Nb ₃ Al	Cubic	<i>cP8</i>	<i>Pm-3n</i>	A15	[14]
“Ti ₄ NbAl ₃ ”, ω_o	Hexagonal	<i>hP6</i>	<i>P6₃/mmc</i>	B8 ₂	[15]
Ti ₂ NbAl, O	Orthorhombic	<i>oC16</i>	<i>Cmcm</i>		[16]

this may be, on the one hand, the partial inconsistency of the available experimental data and, on the other hand, the lack of such data in certain compositional ranges.

The present work investigates the phase equilibria in a series of heat-treated Ti-Al-Nb alloys (with up to 45 at.% Al and 30 at.% Nb) and diffusion couples between 700 and 900 °C. The alloys and diffusion couples are characterized by means of scanning electron microscopy (SEM), electron probe microanalysis (EPMA), x-ray diffraction (XRD), high-energy XRD (HEXRD), transmission electron microscopy (TEM), and differential thermal analysis (DTA). The resulting data are discussed in the context of the information available from the above-mentioned literature, and partial isothermal sections at 700, 800, and 900 °C are established. Phase equilibria at higher temperatures from 1000 to 1300 °C will be presented in another publication.^[36]

2 Experimental

For the investigation of the phase equilibria between 700 and 900 °C, a series of 15 ternary alloys and four single-phase binary alloys (used for diffusion couple experiments) have been synthesized (Table 2 and Fig. 1) by means of an arc-melter with a tiltable crucible in Ar atmosphere. The Ar gas was additionally dried to remove remaining moisture and oxygen (ZPure MTM 3800cc, Chromatography research supplies) to ensure that the impurity levels are as low as possible. Additionally, high purity elements Ti (99.995 wt.%), Al (99.999 wt.%), and Nb (99.9 wt.%) (HMW Hauner GmbH & Co. KG) were used for alloy synthesis. The rod-shaped ingots had a diameter of 15 mm and a length of up to 160 mm weighing between 200–300 g each. For selected alloys, inductively coupled plasma atomic emission spectroscopy (ICP-AES, Optima 8300, Perkin Elmer) and inert gas fusion (Fusionmaster ONH, NCS Germany) were performed before subsequent heat treatments to check the overall composition and impurity levels ensuring that no preferential evaporation or contamination has occurred during synthesis. The results are summarized in Table 2 together with the performed heat treatments for the bulk alloys.

For the heat treatment of bulk alloys, cylinders with 10 mm length were cut from the rods and encapsulated in fused silica ampules backfilled with Ti-gettered Ar gas to minimize contamination uptake during heat treatment. The alloys were heat-treated for 1500, 1000, and 650 h at 700, 800, and 900 °C, respectively, before being quenched in brine by breaking the capsules. After the heat treatment, the overall compositions (measured by EPMA) and impurity levels of selected alloys were checked again. The change in overall composition lies within the measurement

uncertainty of ± 1 % (relative)^[37] for the EPMA measurement. The oxygen content only increased slightly by less than 100 wt. ppm, while the nitrogen content remained below the detection limit of 50 wt. ppm.

For the diffusion couple studies, two different approaches were used: i) solid-solid diffusion couples and ii) liquid-solid diffusion couples. For the solid-solid diffusion couples, blocks (approx. 4 x 4 x 6 mm³) of different binary alloys were cut and their surfaces were ground with SiC paper (220–2500 grit) and cleaned with ethanol. The pieces were then brought into close contact by placing them on top of each other and fixing them with a Mo-clamp to ensure that they remain in contact during the following heat treatment (see Fig. 2). Before the heat treatment, the diffusion couple was encapsulated as described for the bulk alloys. In case of the liquid-solid diffusion couples, cylinders (\varnothing 15 x 4 mm³) of the three binary Ti-Nb alloys were placed in an alumina crucible on top of solid Al-pieces, which are liquid at the heat treatment temperatures of 700 and 800 °C. This ensures that the solid material is surrounded by liquid Al at the beginning of the heat treatment. The crucibles were filled up with Ti filings acting as an oxygen getter. To avoid a direct contact with the diffusion couple, the filings were separated from the diffusion couple by a Ta-foil. This setup (see Fig. 2) was heat-treated in a vacuum furnace at 700 and 800 °C for 100 h, depending on the planned temperature of the following heat-treatment, followed by furnace cooling. Afterwards the diffusion couple was encapsulated as described above and further annealing at 700 and 800 °C was performed until the desired heat treatment durations of 1150 and 750 h were reached. This was possible since enough Ti and Nb had diffused into the Al to form an intermetallic layer with a melting point above the heat treatment temperature. After the heat treatment, the capsules were immediately removed from the furnace, cooled in air, and broken when room temperature was reached. Afterwards the diffusion couples were cut and metallographically prepared. The schematic experimental setup for both types of diffusion couples is shown in Fig. 2, and temperatures and times of the heat treatments for the different combinations are summarized in Table 3.

After metallographic preparation, the microstructures were characterized by SEM and the overall and phase compositions were determined by means of EPMA (JEOL JXY-8100) operated at an acceleration voltage of 15 kV and a probe current of 20 nA. Pure elements were used as standard material. The overall compositions of the heat-treated samples were determined by grid measurements. At least three representative areas of the microstructure were measured with grids (usual step size 20 μ m), each consisting of at least 196-point measurements. These measurements showed that no preferential evaporation of Al

Table 2 Synthesized ternary (B1 to B15) and binary (D1 to D4) alloys with their nominal and measured compositions (ICP-AES) as well as their contents of impurity elements O and C. The N contents

were also analysed, the values were all below the detection limit of 50 wt. ppm and are therefore not listed here. The applied heat treatment times at 700, 800, and 900 °C are given in the last columns

No.	Nominal composition			Measured as-cast composition (ICP-AES)			Impurity contents		Heat treatment time, h		
	Ti, at.%	Al, at.%	Nb, at.%	Ti, at.%	Al, at.%	Nb, at.%	O, wt. ppm	C, wt. ppm	700 °C	800 °C	900 °C
<i>Bulk alloys</i>											
B1	77.5	17.5	5	77.8	17.4	4.8	290	130	1500	1000	650
B2	72.5	17.5	10						1500	1000	650
B3	62.5	20	17.5				220		1500	1000	650
B4	60	25	15	60.5	24.6	14.9	130	110	1500	1000	650
B5	50	25	25								1000
B6	45	30	25								1000
B7	54.5	33	12.5	55.0	32.8	12.2	180	85	1500	1000	650
B8	49	33	17.5	50.3	32.4	17.3	290	120	1500	1000	650
B9	53	37	10	52.8	37.2	10.0	160	86	1500	1000	650
B10	49.5	37	13.5								1000
B11	50	40	10	50.4	39.6	10.0	290	160	1500	1000	650
B12	40	40	20	40.3	39.8	19.9	130	110	1500	1000	650
B13	50	45	5	50.7	43.4	4.9	150	108	1500	1000	650
B14	47.5	45	7.5	48.3	45.8	5.9	140	89	1500	1000	650
B15	42.5	45	12.5	43.0	44.7	12.3	200	102	1500	1000	650
<i>Single-phase alloys for diffusion couple studies</i>											
D1	50	50	0	50.5	49.5	0	160				
D2	80	0	20	80.5	0	19.5					
D3	70	0	30	69.2	0	30.8					
D4	50	0	50	51.3	0	48.7					

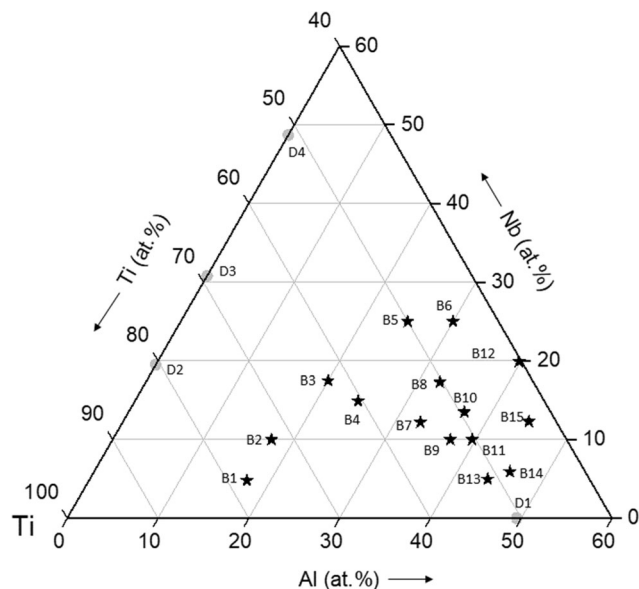


Fig. 1 Alloy composition of the ternary bulk alloys (B1-B15, black stars) and the compositions of the binary single-phase alloys (D1-D4; grey circles) plotted in the Ti-rich corner of the ternary composition space

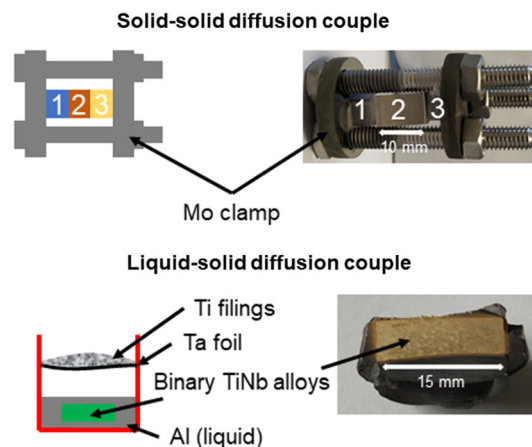


Fig. 2 Schematic setup for solid-solid (top) and liquid-solid (bottom) diffusion couples. On the top right side, the solid-solid diffusion couple is shown before encapsulation (piece 1 is D2 (Ti-20Nb), piece 2 is D1 (Ti-50Al), and piece 3 is D3 (Ti-30Nb)). A solidified liquid-solid diffusion couple after heat treatment is displayed on the bottom right side

Table 3 Overview of investigated diffusion couples

Combination	Type	Temperature	Time
D2-Al	Liquid-solid	700 °C	1150 h
D3-Al	Liquid-solid	700 °C	1150 h
D2-Al	Liquid-solid	800 °C	750 h
D3-Al	Liquid-solid	800 °C	750 h
D4-Al	Liquid-solid	800 °C	750 h
D2-D1-D3	Solid-solid	900 °C	400 h

had occurred during the heat treatments. The chemical composition of the phases was determined by averaging the results of at least 12-point measurements, which were performed in different parts of the sample's cross section. In a few cases where the phases were too small for direct spot analyses (diameters $\leq 1 \mu\text{m}$), the phase compositions were estimated from an extrapolation in a plot of the complete grid measurements which were done for the determination of the overall compositions. In fine lamellar areas, a widened beam was used to determine the average composition of this area. Phase fractions were determined by applying the lever rule for two- and three-phase alloys to the measured values of the overall and phase compositions.

The concentration profiles along the direction of diffusion in the diffusion couples were measured by EPMA line scans with a step size of $1 \mu\text{m}$. These data were used to determine the homogeneity ranges and equilibrium phase compositions of the intermetallic compounds. This is possible because there is local equilibrium at the interfaces of the different diffusion layers.^[38,39] Taking this into account, the composition of the respective phases can be determined by extrapolating to the phase boundaries. At least five line scans are used to determine the chemical composition of the intermetallic phases by averaging of the extrapolated values.

The phases were identified by room temperature XRD and HEXRD as well as in situ HEXRD heating measurements. For the XRD measurements, the samples were crushed into powder, sieved to a grain size $< 90 \mu\text{m}$ and then measured with a Bruker D8 Advanced A25-X1-1 diffractometer using $\text{CoK}\alpha_1$ ($\lambda = 1,78897 \text{ \AA}$) radiation in Bragg-Brentano geometry. A Lynxeye 1D detector was used to measure the intensity of the diffracted beam after passing a Soller collimator with an acceptance angle of 0.3° . The samples were rotated during the measurement to improve grain statistics, and the data were recorded in the range $2\theta = 20^\circ$ to 130° with a step size of 0.01° .

For the in situ HEXRD heating measurements, cuboidal samples ($4 \times 4 \times 10 \text{ mm}^3$) were cut from the heat-treated alloys (usually the samples heat treated at $700 \text{ }^\circ\text{C}/1500 \text{ h}$

were used). The measurements were performed at the High-Energy Materials Science (HEMS) beamline^[40] operated by Hereon at the synchrotron storage ring PETRA III, DESY, Hamburg, Germany. The samples were set up in a modified quenching and deformation dilatometer DIL805A/D from TA Instruments. The measurements were performed under Ar atmosphere. The temperature was controlled with S- and B-type thermocouples spot-welded to the specimen. The specimens were heated up slowly (with 1 or 2 K/min) to ensure near equilibrium conditions. For the room temperature measurements, cylindrical samples with a diameter of 15 mm and varying thickness were used. During the exposure time of 100 s for one diffraction pattern, the samples were slowly rotated by up to 180° to obtain a sufficient grain statistic. For in situ HEXRD and room temperature HEXRD measurements the samples were measured in transmission with a photon energy of 100 keV ($\lambda = 0.124 \text{ \AA}$) and a beam size of 1 mm^2 . The diffraction patterns were recorded with a 2D PerkinElmer flat panel detector XRD 1621. The data were integrated over 360° azimuthal angle using the program Fit2d.^[41] The data is analyzed using the MAUD software package.^[42]

Conventional TEM was carried out using a Philips CM12 instrument operated at 120 kV. The chemical composition of the phases was measured by energy dispersive x-ray spectroscopy (EDS) microanalysis using an EDAX detector system. All specimens for TEM investigations were cut, ground, polished and subsequently electrolytically thinned to electron transparency using electrolyte A3 from Struers.

To investigate the phase transformation temperatures and to complement the experimental results from other methods, DTA measurements were performed using a Netzsch DSC 404C Pegasus thermal analyzer. Calibration was done with certified Al, Au, and Ni standards and the accuracy was regularly checked by melting Al ($660 \text{ }^\circ\text{C}$) and Au ($1064 \text{ }^\circ\text{C}$). As deviations after calibration were $\leq 1 \text{ }^\circ\text{C}$ in all cases, the accuracy of the determined values was estimated to be $\pm 1 \text{ }^\circ\text{C}$. For the measurements, cuboid samples with dimensions of approximately $3 \times 3 \times 2 \text{ mm}$ were cut, cleaned with ethanol, and measured with up to four different heating rates (1, 2, 5, and $10 \text{ }^\circ\text{C}/\text{min}$). Further information including heating and cooling cycles as well as evaluation of the measurement data can be found in Ref. [8].

3 Results

The phase and alloy compositions obtained by the EPMA measurements on heat-treated bulk alloys are summarized in Table 4 through Table 6 at the different investigated temperatures. Additionally, the phase fractions (from

Table 4 EPMA and HEXRD results on phase contents, alloy and phase compositions, phase fractions, and lattice parameters of alloys heat-treated at 700 °C for 1500 h (accuracy of the lattice parameters is ± 0.001 Å, n.d.: not determined)

Alloy no.	Composition after heat treatment, at. %	Phases	Phase compositions measured with EPMA, at. %		Phase fraction, vol. %	Pearson symbol	Lattice parameters, Å		
			Al	Nb			a	b	c
B1	Ti-17.6Al-4.8Nb	(α Ti)	17.0 \pm 1.0(c)	4.3 \pm 1.0(c)	34	<i>hP2</i>	n.d.		n.d.
		(β Ti,Nb)	12.5 \pm 1.0(c)	11.0 \pm 1.0(c)	6	<i>cI2</i>	n.d.		
		Ti ₃ Al	18.4 \pm 1.0(c)	4.5 \pm 1.0(c)	61	<i>hP8</i>	n.d.		n.d.
B2	Ti-18.2Al-9.9Nb	(β Ti,Nb)	10.0 \pm 1.0(d)	18.0 \pm 1.0(d)	30	<i>cI2</i>	n.d.		
		Ti ₃ Al	21.3 \pm 0.4	6.5 \pm 0.3	70	<i>hP8</i>	n.d.		n.d.
B3	Ti-19.4Al-17.4Nb	(β Ti,Nb)	8.1 \pm 0.6	35.4 \pm 0.7	29	<i>cI2</i>	n.d.		
		Ti ₃ Al	23.5 \pm 0.3	10.4 \pm 0.6	71	<i>hP8</i>	n.d.		n.d.
B4	Ti-24.7Al-14.6Nb	Ti ₃ Al	25.2 \pm 1.0(d)	12.4 \pm 1.0(d)	41	<i>hP8</i>	n.d.		n.d.
		O	24.0 \pm 1.0(d)	16.2 \pm 1.0(d)	59	<i>oC16</i>	n.d.	n.d.	n.d.
B7	Ti-32.7Al-11.6Nb	Ti ₃ Al	29.0 \pm 1.0(d)	11.0 \pm 1.0(d)	4(f)	<i>hP8</i>	5.798		4.666
		ω_0	32.9 \pm 1.0(d)	11.6 \pm 1.0(d)	96(f)	<i>hP6</i>	4.581		5.533
B8	Ti-32.8Al-16.8Nb	O	28.0 \pm 1.0(d)	20.0 \pm 1.0(d)	2(f)	<i>oC16</i>	6.055	9.614	4.647
		ω_0	32.9 \pm 0.4	16.7 \pm 1.0	98(f)	<i>hP6</i>	4.587		5.519
B9	Ti-36.4Al-9.7Nb	Ti ₃ Al	35.0 \pm 1.0(d)	9.5 \pm 1.0(d)	(h)	<i>hP8</i>	5.773		4.676
		TiAl	45.0 \pm 1.0(d)	8.0 \pm 1.0(d)	(h)	<i>tP4</i>	4.010		4.075
		ω_0	34.1 \pm 0.6	10.3 \pm 0.4	(h)	<i>hP6</i>	4.578		5.536
B11	Ti-39.8Al-9.4Nb	Ti ₃ Al	35.0 \pm 1.0(d)	9.5 \pm 1.0(d)	5	<i>hP8</i>	n.d.		n.d.
		TiAl	44.7 \pm 0.5	8.0 \pm 0.6	48	<i>tP4</i>	4.017		4.077
		ω_0	35.4 \pm 0.7	10.8 \pm 0.7	47	<i>hP6</i>	4.581		5.530
B12(a)	Ti-39.6Al-20.0Nb	TiAl	43.7 \pm 0.8	17.2 \pm 1.0	50	<i>tP4</i>	4.021		4.080
		ω_0	36.0 \pm 0.7	20.6 \pm 1.1	44	<i>hP6</i>	4.595		5.498
		Nb ₂ Al	33.0 \pm 1.0(e)	37.0 \pm 2.0(e)	6	<i>tP30</i>	n.d.		n.d.
B13(b)	Ti-44.3Al-4.9Nb	Ti ₃ Al	35.7 \pm 0.8	6.8 \pm 0.6	17	<i>hP8</i>	5.735		4.660
		TiAl	46.1 \pm 0.7	4.4 \pm 0.4	83	<i>tP4</i>	4.022		4.066
B14(b)	Ti-45.8Al-5.2Nb	Ti ₃ Al	35.6 \pm 0.6	8.4 \pm 0.3	12	<i>hP8</i>	n.d.		n.d.
		TiAl	46.9 \pm 0.6	5.3 \pm 0.2	88	<i>tP4</i>	n.d.		n.d.
B15(a)	Ti-44.5Al-11.7Nb	TiAl	46.0 \pm 1.1	11.3 \pm 1.4	86	<i>tP4</i>	4.028		4.069
		ω_0	35.0 \pm 0.7	15.2 \pm 0.6	14	<i>hP6</i>	4.587		5.516

(a) Sample contains a small amount (≤ 2 vol.%) of Ti₃Al which is not an equilibrium phase, see section 3

(b) Sample contains a small amount (≤ 1 vol.%) of ω_0 which is not an equilibrium phase, see section 3

(c) Microstructure too fine (particles $< 1\mu\text{m}$) to determine phase composition by single spot EPMA measurements; phase composition approximated with the help of grid measurements

(d) Phase compositions approximated taking into account tie-line data from nearby alloys and diffusion couples and/or phase fractions from HEXRD measurements, see section 3

(e) Phase composition is estimated, see section 3

(f) Phase fractions determined with HEXRD

(h) Reliable phase fractions cannot be determined because of small phase fraction and estimated composition value

EPMA if not indicated otherwise) and measured lattice parameters (from HEXRD if not indicated otherwise) of all phases are provided. The results of the diffusion couple experiments are listed in Table 7. The compositions given in the following text together with the alloy designations are always those measured in the as-cast condition. The

actual overall compositions of the heat-treated samples are given in the respective Tables 4, 5, and 6 and may slightly differ from the as-cast values.

Alloy B1 (Ti-17.4Al-4.8Nb) exhibits a three-phase microstructure at all three temperatures investigated, as can be seen in Fig. 3(a)-(c). The phases present were identified

Table 5 EPMA and HEXRD results on phase contents, alloy and phase compositions, phase fractions, and lattice parameters of alloys heat-treated at 800 °C for 1000 h (accuracy of the lattice parameters is ± 0.001 Å, n.d.: not determined)

Alloy No.	Composition after heat treatment, at.%	Phases	Phase compositions measured with EPMA, at.%		Phase fraction, vol.%	Pearsonsymbol	Lattice parameters, Å		
			Al	Nb			a	b	c
B1	Ti-17.5Al-4.7Nb	(αTi)	17.0 ± 1.0(c)	4.3 ± 1.0(c)	35	hP2	2.929	4.678	
		(βTi,Nb)	11.6 ± 1.0(c)	10.8 ± 1.0(c)	4	cI2	(f)		
		Ti ₃ Al	18.1 ± 1.0(c)	4.6 ± 1.0(c)	60	hP8	5.808	4.667	
B2	Ti-18.1Al-9.5Nb	(βTi,Nb)	10.6 ± 0.7	15.6 ± 0.7	36	cI2	(f)		
		Ti ₃ Al	22.3 ± 0.3	6.1 ± 0.2	64	hP8	5.801	4.667	
B3	Ti-20.2Al-16.3Nb	(βTi,Nb)	11.8 ± 0.5	28.1 ± 0.8	33	cI2	n.d.		
		Ti ₃ Al	24.1 ± 0.1	10.9 ± 0.4	67	hP8	n.d.	n.d.	
B4	Ti-24.9Al-14.1Nb	Ti ₃ Al	25.5 ± 1.0(c)	12.3 ± 1.0(c)	44	hP8	5.804	4.657	
		O	24.5 ± 0.3	15.5 ± 0.9	56	oC16	5.946	9.779	4.669
B7	Ti-32.3Al-11.8Nb	Ti ₃ Al	29.0 ± 1.0(c)	11.0 ± 1.0(c)	5(e)	hP8	5.785	4.669	
		ω _o	32.5 ± 1.0(c)	11.8 ± 1.0(c)	95(e)	hP6	4.579	5.527	
B8	Ti-32.7Al-17.0Nb	Ti ₃ Al	27.0 ± 1.0(d)	12.0 ± 1.0(d)	1(e)	hP8	n.d.	n.d.	
		O	28.0 ± 1.0(d)	20.0 ± 1.0(d)	5(e)	oC16	6.065	9.621	4.662
		ω _o	32.9 ± 1.0(d)	17.0 ± 1.0(d)	94(e)	hP6	4.587	5.510	
B9	Ti-36.1Al-9.7Nb	Ti ₃ Al	34.5 ± 1.0(d)	9.5 ± 1.0(d)	(g)	hP8	n.d.	n.d.	
		TiAl	45.0 ± 1.0(d)	7.7 ± 1.0(d)	(g)	tP4	n.d.	n.d.	
		ω _o	34.8 ± 0.8	10.0 ± 0.6	(g)	hP6	n.d.	n.d.	
B11	Ti-39.5Al-9.5Nb	Ti ₃ Al	34.5 ± 1.0(d)	9.5 ± 1.0(d)	3	hP8	5.757	4.676	
		TiAl	44.9 ± 1.1	7.4 ± 0.4	47	tP4	4.017	4.071	
		ω _o	34.6 ± 0.8	11.5 ± 0.5	50	hP6	4.579	5.528	
B12(a)	Ti-39.9Al-19.3Nb	TiAl	45.3 ± 0.1	16.6 ± 0.4	46	tP4	4.076	4.080	
		ω _o	35.0 ± 0.9	20.6 ± 0.6	46	hP6	4.595	5.497	
		Nb ₂ Al	37.0 ± 0.5	27.7 ± 0.4	8	tP30	9.927	5.131	
B13(b)	Ti-43.5Al-5.1Nb	Ti ₃ Al	33.2 ± 0.6	8.2 ± 0.3	18	hP8	5.752	4.652	
		TiAl	45.6 ± 0.2	4.8 ± 0.1	82	tP4	4.020	4.064	
B14	Ti-44.4Al-6.0Nb	Ti ₃ Al	34.1 ± 0.9	9.2 ± 0.4	11	hP8	n.d.	n.d.	
		TiAl	45.6 ± 0.4	5.7 ± 0.2	89	tP4	n.d.	n.d.	
B15(a)	Ti-43.3Al-12.2Nb	TiAl	45.9 ± 0.4	10.6 ± 0.5	79	tP4	4.023	4.068	
		ω _o	33.5 ± 0.6	16.9 ± 0.6	21	hP6	4.584	5.511	

- (a) Sample contains a small amount (≤ 2 vol.%) of Ti₃Al which is not an equilibrium phase, see section 3
- (b) Sample contains a small amount (≤ 1 vol.%) of ω_o which is not an equilibrium phase., see section 3
- (c) Microstructure too fine (particles < 1μm) to determine phase composition by single spot EPMA measurements; phase composition approximated with the help of grid measurements
- (d) Phase compositions approximated taking into account tie-line data from nearby alloys and diffusion couples and/or phase fractions from HEXRD measurements, see section 3
- (e) Phase fractions determined with HEXRD
- (f) (βTi,Nb) transformed to α'' martensite during quenching. Therefore, no lattice parameters could be determined for (βTi,Nb)
- (g) Reliable phase fractions cannot be determined because of small phase fraction and estimated composition value

to be (αTi), (βTi,Nb), and Ti₃Al by HEXRD measurements of quenched samples.

In alloys B2 (Ti-17.5Al-10Nb) and B3 (Ti-20Al-17.5Nb), a two-phase microstructure (βTi,Nb) + Ti₃Al is observed after heat treatments at 700 to 900 °C . This was

also confirmed by room-temperature HEXRD on the quenched samples and in addition by in situ HEXRD for alloy B2. The microstructures of the heat-treated alloys B2 and B3 show large (βTi,Nb) grains with Ti₃Al at the grain boundaries and small Ti₃Al precipitates inside the grains

Table 6 EPMA and HEXRD results on phase contents, alloy and phase compositions, phase fractions, and lattice parameters of alloys heat-treated at 900 °C for 650 h (1000 h in case of B5, B6, and B10) (accuracy of the lattice parameters is ± 0.001 Å, n.d.: not determined)

Alloy no.	Composition after heat treatment, at.%	Phases	Phase compositions measured with EPMA, at.%		Phase fraction, vol.%	Pearson symbol	Lattice parameters, Å		
			Al	Nb			a	b	c
B1	Ti-17.7Al-4.7Nb	(α Ti)	17.6 \pm 0.5	3.7 \pm 0.1	49	<i>hP2</i>	2.917		4.675
		(β Ti,Nb)	13.3 \pm 0.2	8.1 \pm 0.2	22	<i>cI2</i>	(f)		
		Ti ₃ Al	21.1 \pm 0.5	3.9 \pm 0.2	29	<i>hP8</i>	5.805		4.667
B2	Ti-17.5Al-10Nb(d)	(β Ti,Nb)	12.8 \pm 0.2	13.2 \pm 0.2	53	<i>cI2</i>	(f)		
		Ti ₃ Al	22.2 \pm 0.4	6.2 \pm 0.4	47	<i>hP8</i>	5.798		4.666
B3	Ti-20Al-17.5Nb(d)	(β Ti,Nb)	15.3 \pm 0.5	22.1 \pm 0.4	56	<i>cI2</i>	n.d.		
		Ti ₃ Al	23.7 \pm 0.5	11.1 \pm 0.2	44	<i>hP8</i>	n.d.		n.d.
B4	Ti-24.8Al-14.5Nb	(β Ti,Nb) _o	16.9 \pm 0.1	23.6 \pm 0.2	3	<i>cP2</i>	3.261		
		Ti ₃ Al	25.0 \pm 0.2	12.7 \pm 0.6	17	<i>hP8</i>	5.796		4.664
		O	25.0 \pm 0.1	14.6 \pm 0.5	80	<i>oC16</i>	5.945	9.780	4.668
B5	Ti-23.5Al-26.7Nb	(β Ti,Nb)	16.8 \pm 0.7	33.5 \pm 0.7	18	<i>cI2</i>	3.261		
		O	25.3 \pm 0.1	24.3 \pm 0.5	82	<i>oC16</i>	6.065	9.600	4.670
B6(a)	Ti-28.9Al-25.3Nb	O	28.8 \pm 0.6	24.9 \pm 1.3	96	<i>oC16</i>	6.11(g)	9.53(g)	4.65(g)
		Nb ₂ Al	32.6 \pm 0.3	31.7 \pm 0.7	4	<i>tP30</i>	9.94(g)		5.14(g)
	Ti-30.3Al-22.5Nb	Ti ₃ Al	29.2 \pm 0.6	12.5 \pm 0.9	20	<i>hP8</i>	5.78(g)		4.67(g)
		O	28.2 \pm 0.8	20.2 \pm 0.9	40	<i>oC16</i>	6.11(g)	9.53(g)	4.65(g)
B7	Ti-33.2Al-11.7Nb	Nb ₂ Al	33.0 \pm 0.4	30.0 \pm 0.8	40	<i>tP30</i>	9.94(g)		5.14(g)
		Ti ₃ Al	32.8 \pm 0.7	9.0 \pm 0.4	42	<i>hP8</i>	5.779		4.651
		ω_o	33.5 \pm 0.2	12.4 \pm 0.5	58	<i>hP6</i>	4.579		5.527
		Ti ₃ Al	30.7 \pm 0.2	12.8 \pm 0.3	8	<i>hP8</i>	5.785		4.664
B8(b)	Ti-32.6Al-16.9Nb	O	30.5 \pm 0.2	17.9 \pm 0.4	20	<i>oC16</i>	6.065	9.600	4.662
		ω_o	33.4 \pm 0.4	17.1 \pm 0.4	72	<i>hP6</i>	4.580		5.534
		Ti ₃ Al	34.6 \pm 0.8	8.3 \pm 0.2	57	<i>hP8</i>	5.775		4.643
B9	Ti-36.6Al-9.0Nb	TiAl	45.1 \pm 0.3	7.8 \pm 0.1	19	<i>tP4</i>	4.026		4.061
		ω_o	34.3 \pm 0.8	11.7 \pm 0.3	24	<i>hP6</i>	4.576		5.538
		Ti ₃ Al	35.0 \pm 0.2(e)	13.9 \pm 0.2(e)	80	<i>cP2</i>	3.222		
B10(c)	Ti-37Al-13.5Nb(d)	TiAl	45.2 \pm 0.5	9.6 \pm 0.2	15	<i>tP4</i>	4.010		4.054
		ω_o	35.0 \pm 0.2(e)	13.9 \pm 0.2(e)	5	<i>hP6</i>	n.d.		n.d.
		Ti ₃ Al	35.9 \pm 0.5	8.4 \pm 0.2	1	<i>hP8</i>	5.775		4.643
B11	Ti-39.5Al-9.3Nb	TiAl	45.3 \pm 0.3	8.0 \pm 0.2	47	<i>tP4</i>	4.027		4.063
		ω_o	34.1 \pm 0.6	10.5 \pm 0.4	52	<i>hP6</i>	4.576		5.533
		TiAl	45.4 \pm 0.6	11.4 \pm 0.8	47	<i>tP4</i>	4.025		4.067
B12(c)	Ti-40.0Al-20.3Nb	Nb ₂ Al	35.6 \pm 0.6	28.5 \pm 0.8	53	<i>tP30</i>	9.921		5.133
		Ti ₃ Al	35.4 \pm 0.4	5.3 \pm 0.3	25	<i>hP8</i>	5.769		4.649
B13	Ti-43.4Al-4.9Nb	TiAl	45.8 \pm 0.6	5.1 \pm 0.3	75	<i>tP4</i>	4.027		4.066
		Ti ₃ Al	36.5 \pm 0.5	6.1 \pm 0.2	6	<i>hP8</i>	n.d.		n.d.
B14	Ti-45.8Al-5.9Nb	TiAl	46.4 \pm 0.2	5.8 \pm 0.3	94	<i>tP4</i>	n.d.		n.d.
		TiAl	45.3 \pm 0.5	11.8 \pm 0.5	94	<i>tP4</i>	4.030		4.067
B15(c)	Ti-44.7Al-12.3Nb	ω_o	34.5 \pm 0.3	17.6 \pm 0.3	6	<i>hP6</i>	4.589		5.516

(a) Sample consists of two parts with different composition, see section 3

(b) Furnace temperature must have been slightly below 900 °C; observed phases belong to the equilibrium state below 897 °C, at which temperature the transition reaction (β Ti,Nb)_o + Ti₃Al \rightleftharpoons O + ω_o takes place, see section 3 and 4.2.5

(c) Sample contains a small amount of Ti₃Al, which is not an equilibrium phase, see section 3

(d) Alloy composition after heat treatment not determined; therefore, the nominal composition of the alloy is given, which is also used to determine the phase fractions

(e) (β Ti,Nb)_o and ω_o compositions cannot be distinguished

(f) (β Ti,Nb) transformed to α' martensite during quenching. Therefore, no lattice parameters could be determined for (β Ti,Nb)

(g) HEXRD averages the slightly different lattice parameters of the two regions, which is why the accuracy here is one order of magnitude lower

(Fig. 4a and b), which have the same composition. The extension and position of the $(\beta\text{Ti,Nb}) + \text{Ti}_3\text{Al}$ two-phase field are confirmed by the diffusion couple experiments in the entire temperature range (Table 7).

The extension and position of the $(\beta\text{Ti,Nb}) + \text{Ti}_3\text{Al}$ two-phase field are confirmed by the diffusion couple experiments in the entire temperature range (Table 7). Figure 5(a) shows a typical BSE image of a diffusion zone in a $(\beta\text{Ti,Nb})/\text{TiAl}$ diffusion couple. The measured concentration profile obtained by an EPMA scan along the line indicated in the BSE image is presented in Fig. 5(b). An enlarged view of this concentration profile (Fig. 5c) shows the region of the $(\beta\text{Ti,Nb})/\text{Ti}_3\text{Al}$ interface with the respective steps in the Al and Nb gradients and the extrapolations to the equilibrium phase compositions (see section 2 Experimental).

In alloys B4 to B6, the ternary O phase occurs as equilibrium phase. After heat treatment at 900 °C, alloy B4 (Ti-24.6Al-14.9Nb) exhibits a three-phase microstructure (Fig. 6a) consisting of the bright $(\beta\text{Ti,Nb})_o$ phase (whose B2-ordering was confirmed by in situ HEXRD) and large O phase grains (grey) with fine, mostly plate-like Ti_3Al precipitates (black) inside. On a TEM bright-field image (Fig. 6b) of a respective grain, the plate-like morphology of the Ti_3Al precipitates is well visible, also indicating the existence of an orientation relationship between the two phases. The compositional differences were confirmed by TEM-EDS and in some parts of the microstructure the phases were big enough to be measured by EPMA. Furthermore, the in situ HEXRD measurements show that the $(\beta\text{Ti,Nb})_o$ phase appears at about 880 °C during heating. These results confirm the observations made in the

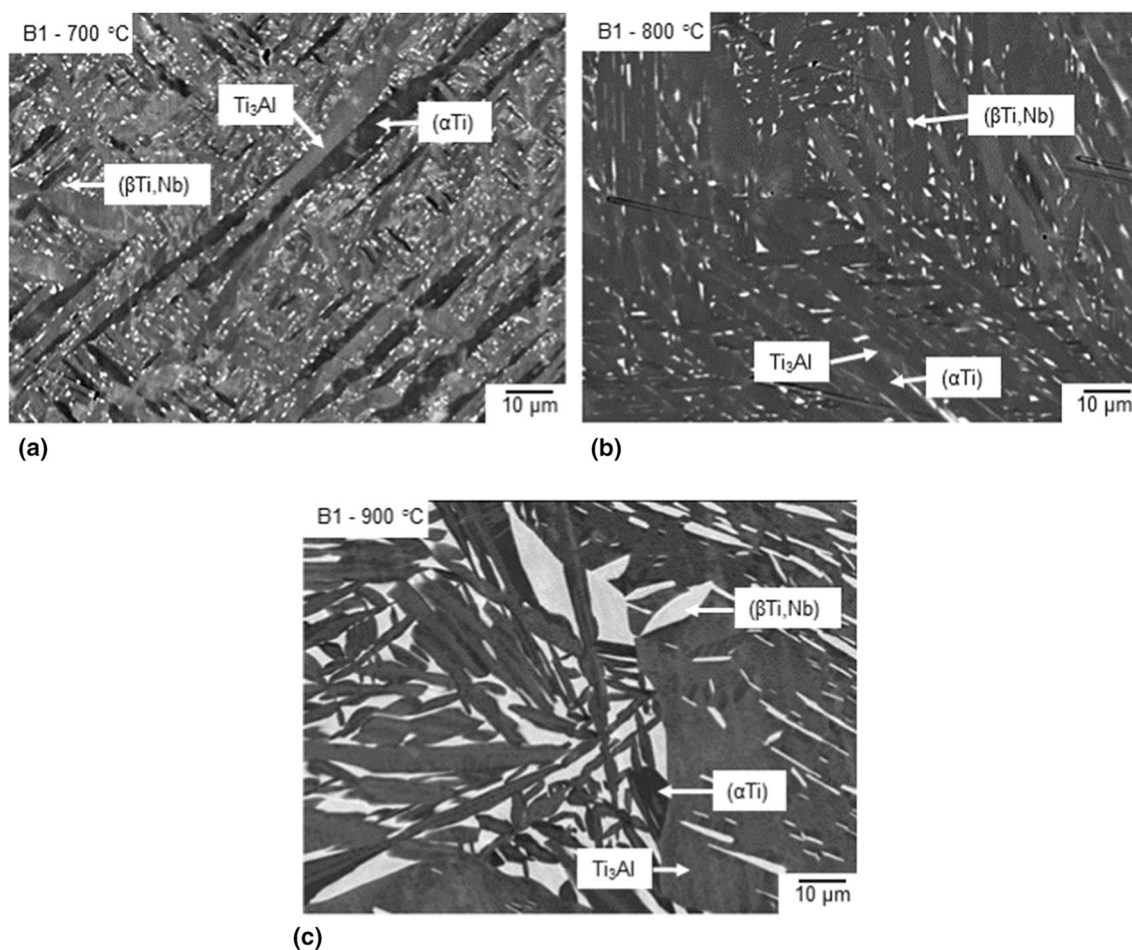


Fig. 3 Back-scattered electron (BSE) images of alloy B1 (Ti-17.4Al-4.8Nb) heat-treated at (a) 700 °C/1500 h, (b) 800 °C/1000 h, (c) 900 °C/650 h showing a three-phase microstructure of (αTi) (grey), $(\beta\text{Ti,Nb})$ (bright), and Ti_3Al (dark)

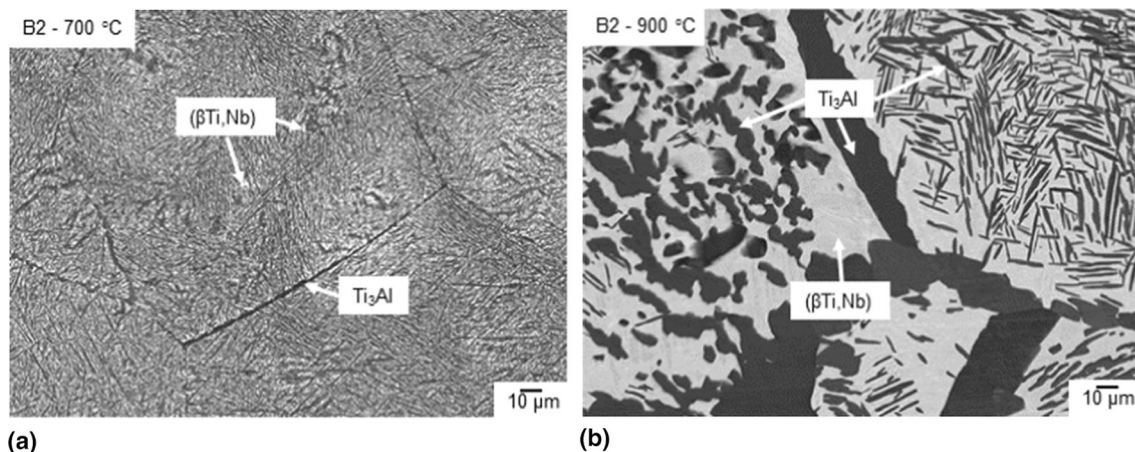


Fig. 4 BSE images of the microstructure of alloy B2 (Ti-17.5Al-10Nb) heat-treated at (a) 700 °C for 1500 h and (b) 900 °C for 650 h with (βTi,Nb) (bright) and Ti₃Al (dark)

Table 7 Extrapolated equilibrium compositions as obtained from the diffusion couples 700 °C/1150 h, 800 °C/750 h, and 900 °C/400 h

Temperature, °C)	Diffusion couple	Phases	Phase compositions determined from line scans, at.%			
			Phase 1		Phase 2	
			Al	Nb	Al	Nb
700	D2-Al(path 1)(a)	(βTi,Nb) + Ti ₃ Al	10.0 ± 1.0	19.0 ± 1.0	20.6 ± 0.5	8.4 ± 0.5
		Ti ₃ Al + TiAl	34.4 ± 0.3	6.8 ± 0.6	46.7 ± 1.1	3.2 ± 1.1
700	D3-Al(path 2)(a)	(βTi,Nb) + O	7.5 ± 2.0	39.5 ± 2.0	25.0 ± 2.0	21.0 ± 2.0
		O + ω _o	28.0 ± 2.0	17.0 ± 2.0	(b)	(b)
		ω _o + TiAl	(b)	(b)	44.0 ± 2.0	9.0 ± 2.0
700	D3-Al	(βTi,Nb) + Ti ₃ Al	6.5 ± 0.7	35.5 ± 1.7	24.0 ± 0.5	10.8 ± 0.5
		Ti ₃ Al + ω _o	26.2 ± 1.0	10.8 ± 1.9	33.0 ± 2.0	11.8 ± 2.0
		ω _o + TiAl	35.0 ± 2.0	13.0 ± 2.0	48.0 ± 2.0	9.5 ± 2.0
800	D2-Al	(βTi,Nb) + Ti ₃ Al	9.9 ± 0.1	17.0 ± 0.3	22.3 ± 1.0	6.4 ± 0.2
		Ti ₃ Al + TiAl	35.8 ± 0.3	6.2 ± 0.2	46.2 ± 0.4	4.2 ± 0.3
800	D3-Al	(βTi,Nb) + Ti ₃ Al	11.4 ± 0.1	29.9 ± 0.8	24.8 ± 0.6	11.3 ± 0.6
		Ti ₃ Al + ω _o	27.7 ± 0.3	11.4 ± 0.1	33.6 ± 0.2	13.9 ± 0.6
		ω _o + TiAl	35.4 ± 0.5	13.1 ± 0.4	45.5 ± 0.1	7.7 ± 0.4
800	D4-Al	(βTi,Nb) + O	11.5 ± 0.4	48.5 ± 0.6	25.5 ± 0.4	28.0 ± 0.7
		O + Nb ₂ Al	27.0 ± 0.6	25.8 ± 0.6	30.3 ± 0.3	39.2 ± 0.8
		Nb ₂ Al + TiAl	37.2 ± 1.0	31.1 ± 0.1	49.0 ± 0.4	18.9 ± 0.6
900	D2-D1	(βTi,Nb) + Ti ₃ Al	14.2 ± 0.6	11.2 ± 0.3	21.5 ± 0.6	4.4 ± 0.5
		Ti ₃ Al + TiAl	36.0 ± 0.4	0.0 ± 0.5	47.2 ± 1.0	0.0 ± 0.2
900	D3-D1	(βTi,Nb) + Ti ₃ Al	14.7 ± 0.1	18.1 ± 0.6	23.7 ± 0.6	8.4 ± 0.8
		Ti ₃ Al + TiAl	36.3 ± 0.3	0.0 ± 0.5	46.7 ± 0.5	0.0 ± 0.2

(a) Two different diffusion paths are observed in this diffusion couple. Because of the sometimes very thin diffusion zones, the accuracy of the extrapolated compositions is reduced to ± 2.0 at.% in some cases

(b) Diffusion layer too thin to perform a reliable extrapolation to the interfaces with the O phase and TiAl

microstructure of alloy B4, where (βTi,Nb)_o is only present at 900 °C, while at 700 and 800 °C the alloy is two-phase Ti₃Al + O.

Alloy B5 (Ti-25Al-25Nb) was heat-treated at 900 °C for 1000 h revealing a two-phase equilibrium between (βTi,Nb) and the O phase. The phases were identified by

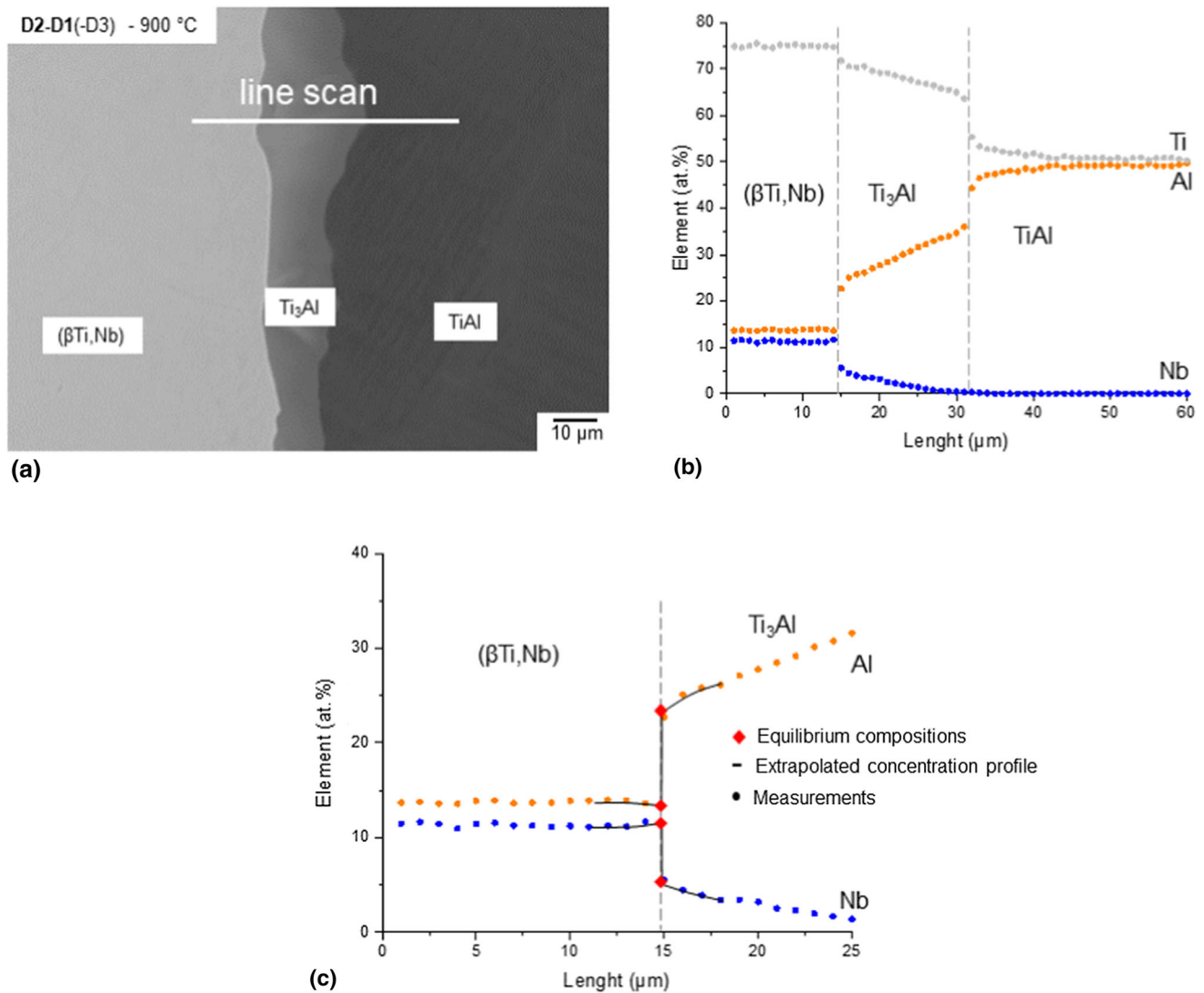


Fig. 5 (a) BSE image of the D2-D1 diffusion zone in diffusion couple D2-D1-D3 heat-treated at 900 °C for 400 h; (b) concentration profile measured along the white line in a); (c) enhanced view showing

the region of the (βTi,Nb)/Ti₃Al interface of the concentration profile with the extrapolated values of the equilibrium phase compositions (red diamonds) (Color figure online)

room-temperature HEXRD measurements. No heat treatments were performed with this alloy at lower temperatures, but the diffusion couple experiments of D3-Al confirm the existence of a (βTi,Nb) + O two-phase field at 700 and 800 °C (Table 7).

Alloy B6 (Ti-30Al-25Nb) with a 5 at.% higher Al content than B5 was also heat-treated at 900 °C for 1000 h. Its composition lies on the Al-rich side of the O phase field. In the metallographic cross section of this sample, some macroscopic inhomogeneity was observed as indicated by the occurrence of two different kinds of microstructure (Fig. 7). Respective EPMA grid measurements confirmed slightly different overall compositions in the two regions. While the Al-lean region consists of a two-phase

microstructure of O phase and Nb₂Al, the Al-rich region additionally contains significant amounts of Ti₃Al (see Table 6). The existence of these phases is confirmed by HEXRD measurements.

The microstructure of alloy B8 (Ti-32.4Al-17.3Nb) appears to be three-phase after the heat treatment at 900 °C (Fig. 7d), and HEXRD of the quenched sample identifies the phases Ti₃Al, O, and ω_o. Although these are the expected equilibrium phases up to slightly lower temperatures (more precisely: up to 897 °C, see section 4.2.5), this does not correspond to the true equilibrium at 900 °C, which instead should be (βTi,Nb)_o + Ti₃Al + ω_o. As is discussed in detail in section 4.2.5, some reactions occur just below 900 °C, and most likely the true heat treatment

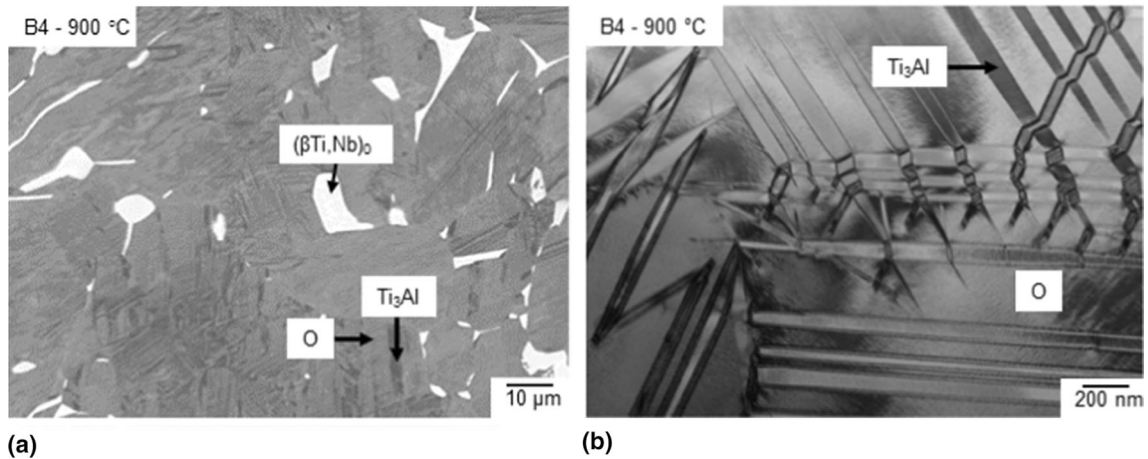


Fig. 6 (a) BSE image of alloy B4 (Ti-24.6Al-14.9Nb) heat-treated at 900 °C/650 h with $(\beta\text{Ti,Nb})_0$ (bright), Ti_3Al (dark), and O phase

(grey) and; (b) Bright field TEM image of the matrix of alloy B4 showing plate-like Ti_3Al in an O phase matrix

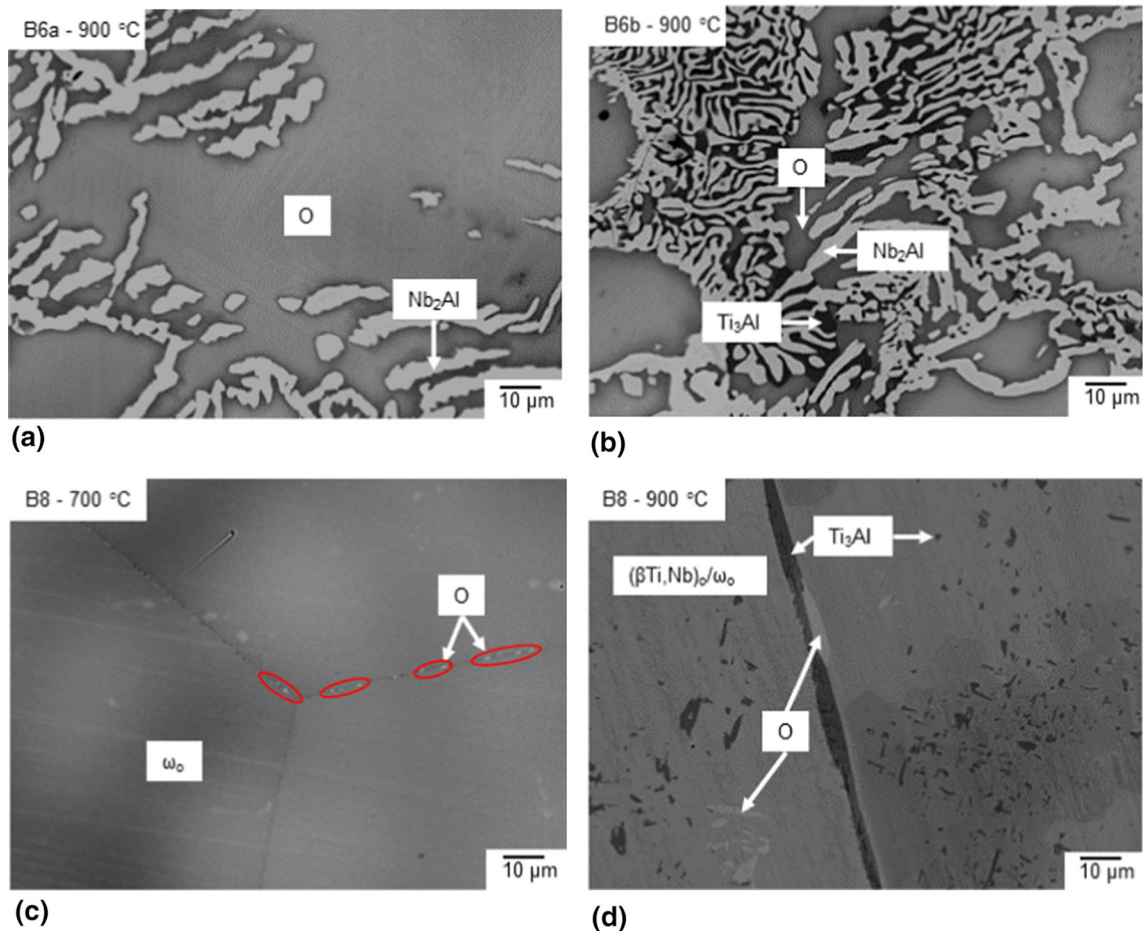


Fig. 7 BSE images of alloy B6 heat-treated at 900 °C/1000 h. The sample consists of two parts representing (a) the two-phase field O + Nb_2Al (Ti-28.9Al-25.3Nb) and (b) the three-phase field Ti_3Al + O + Nb_2Al (Ti-30.3Al-22.5Nb). BSE images of alloy B8 (Ti-32.4Al-17.6Nb) (c) heat-treated at 700 °C/1500 h mainly consisting of ω_0 grains with very small amounts of O phase present (inside the red

circles; bright spots in the ω_0 phase are artefacts from sample preparation) and (d) heat-treated at 900 °C/650h consisting of big $(\beta\text{Ti,Nb})_0/\omega_0$ grains, O (bright) and Ti_3Al (dark), which is a result of the complex reaction sequence close to the heat-treatment temperature and does not represent the true phase equilibrium (see paragraph on alloy B8)

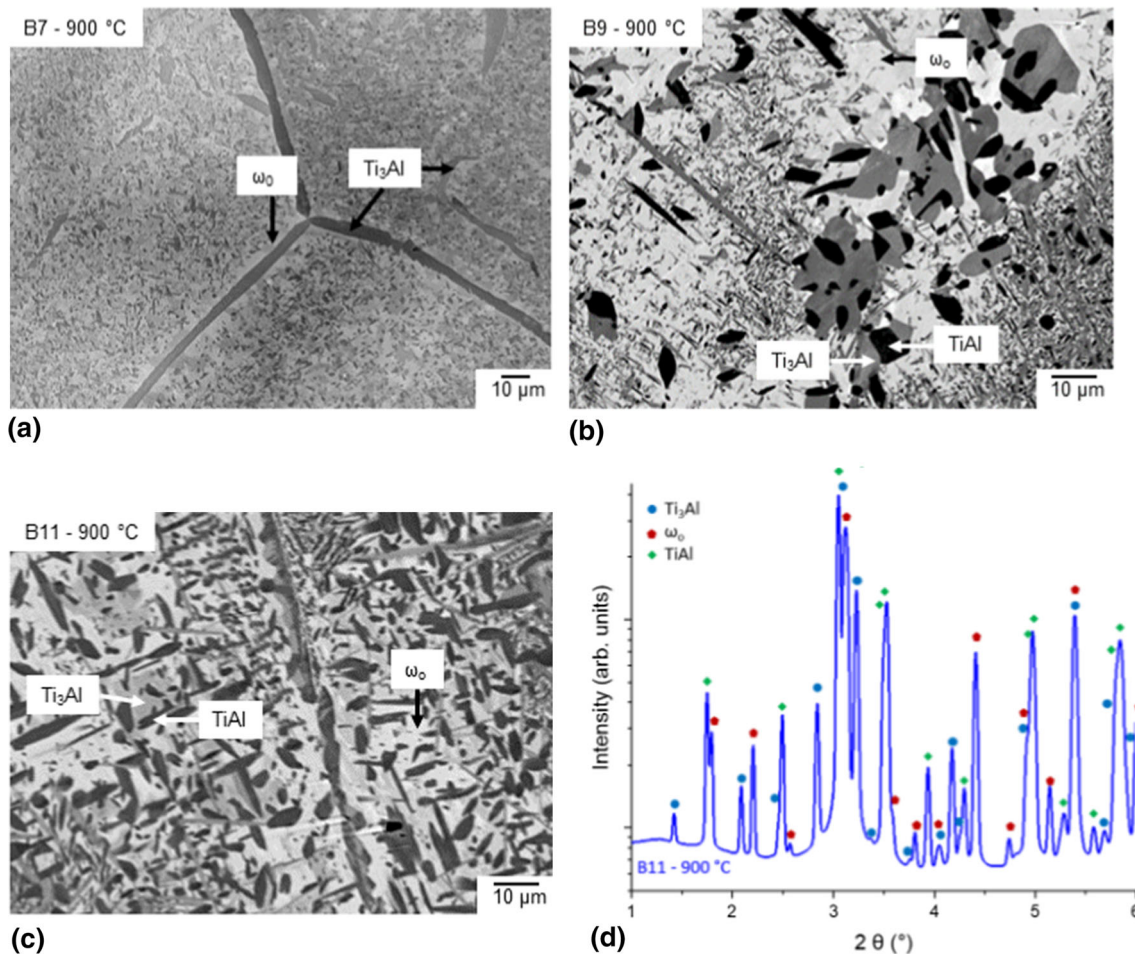


Fig. 8 BSE image of (a) alloy B7 (Ti-32.8Al-12.2Nb) heat-treated at 900 °C with large ω_0 grains (bright) as matrix phase and Ti_3Al (dark) as grain boundary phase and inside the grains as precipitates (the contrast differences appearing in the ω_0 matrix are not due to chemical differences, which was verified by EPMA spot analyses at different positions resulting in identical compositions); (b) alloy B9

(Ti-37.2Al-10.0Nb) and (c) alloy B11 (Ti-39.6Al-10.0Nb) heat-treated at 900 °C for 650 h lying in the same three-phase field composed of Ti_3Al (grey), $TiAl$ (dark), and ω_0 (bright), (d) respective HEXRD pattern (with logarithmic intensity scale) confirming the microstructural results

temperature for this sample was slightly below 900 °C (e.g., 896 °C would be already sufficient), which could explain the observed microstructure. At 700 and 800 °C, the microstructure is almost single-phase ω_0 (Fig. 7c). HEXRD measurements reveal that an additional 5 vol.% O phase and 1 vol.% Ti_3Al are present at 800 °C and 2 vol.% O phases at 700 °C. Due to the low phase fractions and the smallness of the particles, the composition of these phases cannot be measured directly by EPMA, and grid measurements also do not provide reliable values for the phase compositions. However, using the tie-line data from the diffusion couple experiments (D3-Al) and the phase fractions determined by HEXRD, the position of the tie-triangle $Ti_3Al + O + \omega_0$ at 800 °C and the tie-line $O + \omega_0$ at 700 °C can be approximated. This is possible under the assumption that tie-lines located close to tie-triangles are parallel and of similar length to the respective side of this

tie-triangle. Using this approximation, it is possible to roughly estimate the phase compositions (Tables 4 and 5). By applying the lever rule, the obtained compositions can then be checked for agreement with the phase fractions determined by HEXRD.

The same method was used to determine the phase compositions in alloy B7 (Ti-32.8Al-12.2Nb) at 700 and 800 °C, where the microstructure again almost exclusively consists of the ω_0 phase with 4–5 vol.% of Ti_3Al . At 900 °C, the two microstructure constituents are large enough to be measured with EPMA. Figure 8(a) shows the microstructure at 900 °C with Ti_3Al both as grain boundary phase and as precipitates within large ω_0 grains.

Both alloys B9 (Ti-37.2Al-10.0Nb) and B11 (Ti-39.6Al-10.0Nb) show the three-phase equilibrium $Ti_3Al + TiAl + \omega_0$ in the entire studied temperature range from 700 to 900 °C. The respective three-phase microstructures of the

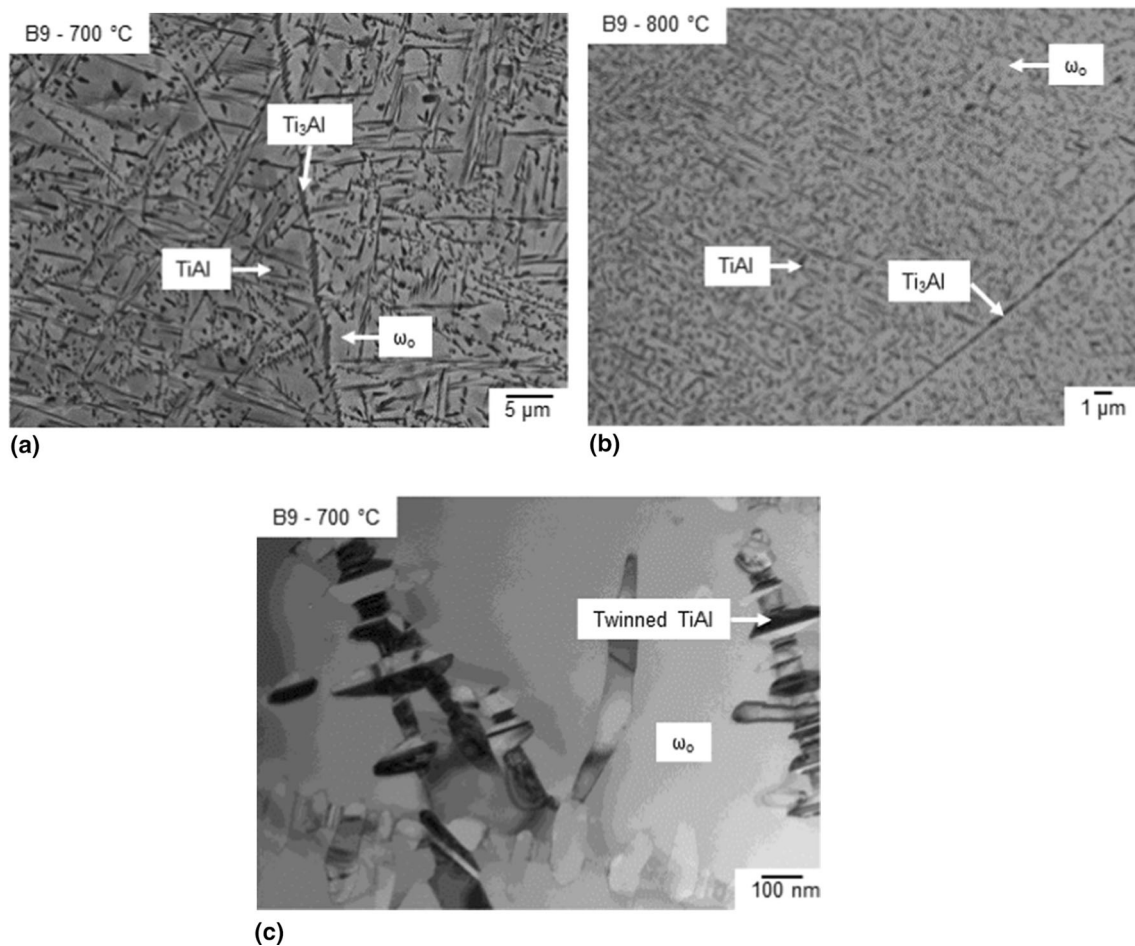


Fig. 9 BSE images of alloy B9 (Ti-37.2Al-10.0Nb) at (a) 700 °C heat-treated for 1500 h and (b) 800 °C heat-treated for 1000 h; both showing a three-phase microstructure between ω_o (grey) as matrix

phase with fine TiAl precipitates and Ti₃Al at the grain boundaries; (c) bright field TEM image of the ω_o matrix with twinned TiAl precipitates identified by SAED

two alloys at 900 °C are shown in Fig. 8(b) and (c). Since the compositions of the two alloys are different, the phase fractions change significantly, which is also visible in the microstructure. The phases were identified by room temperature HEXRD measurements (Fig. 8d). Additionally, in situ HEXRD measurements of alloy B11 prove that ω_o is present in the entire temperature range from 700 to 900 °C before it transforms to (βTi,Nb)_o at a temperature above 900 °C. This was confirmed by DTA investigations,^[8] which give equilibrium transformation onset temperatures of 908 and 906 °C for alloys B9 and B11 (corresponding to alloy A4 and A3 in Ref. [8]).

At 700 and 800 °C, the microstructure of both alloys B9 and B11 is very fine-scaled (Fig. 9). HEXRD measurements confirm the three phases Ti₃Al, TiAl, and ω_o. Large ω_o grains make up the largest part of the microstructure. Small amounts of Ti₃Al have precipitated along the grain boundaries, while the very fine, plate-like precipitates in the grains are TiAl (as was confirmed by TEM selected

area diffraction on alloy B9 heat-treated at 700 °C) with a lot of twins visible in the TEM bright field image Fig. 9(c). Because of the small phase fraction and size of Ti₃Al, it was not possible to measure its composition by EPMA. Therefore, the composition of Ti₃Al at 700 and 800 °C was tentatively estimated using Ti₃Al phase boundary data from the nearby alloys B7, B13 and B14.

Alloy B10 (Ti-37Al-13.5Nb) was heat-treated at 900 °C only. It has a similar Al content as the three-phase alloys B9 and B11 but an about 4 at.% higher Nb content. XRD shows that this alloy contains large amounts of (βTi,Nb)_o and TiAl as well as some ω_o phase, see Fig. 10(a). The microstructure of the quenched sample shows large grains of (βTi,Nb)_o/ω_o (which cannot be distinguished because of their almost identical composition) and TiAl precipitates both inside the grains and on the grain boundaries. In addition, there is a small amount of another phase with lower Nb content, which most likely is some untransformed Ti₃Al. The presence of metastable phases in the

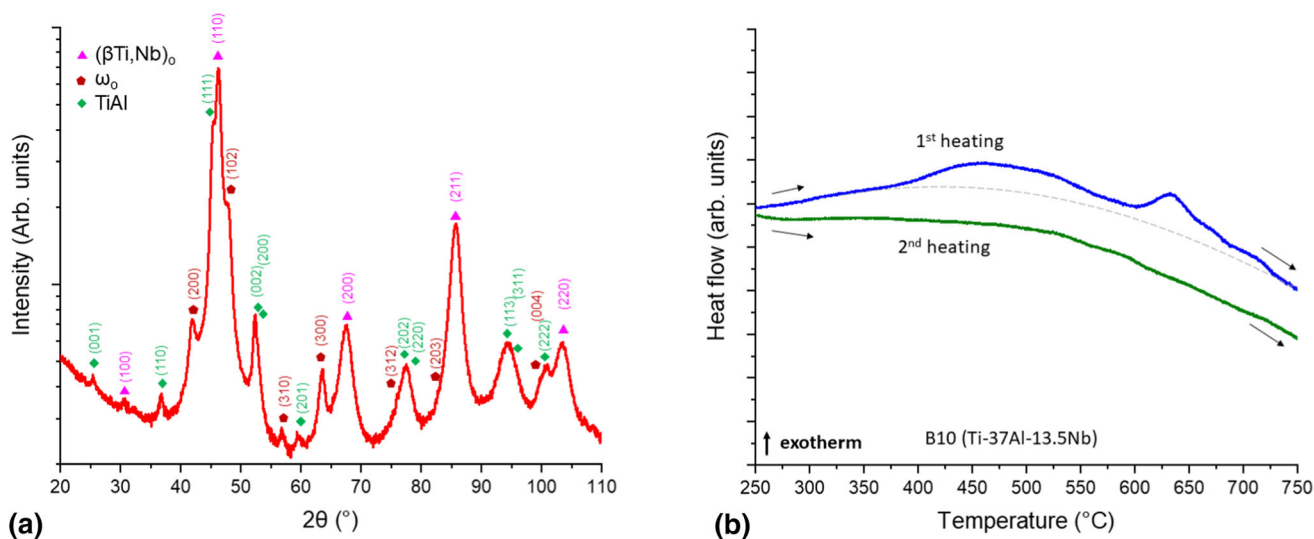


Fig. 10 (a) X-ray diffractogram of alloy B10 (Ti-37Al-13.5Nb) after heat-treatment at 900 °C for 650 h and quenching showing the presence of $(\beta\text{Ti,Nb})_0$, TiAl as well as some ω_0 phase; (b) DTA heating curves of the same sample. The upper curve shows the heat flow signal during first heating (up to 1350 °C) of the quenched

sample, and the lower curve is the result of a second heating of the same sample after cooling from 1350 °C. The exothermic effects during first heating reveal the metastability of the sample quenched from 900 °C (the dashed gray line is to indicate the course of the hypothetical baseline)

quenched sample is confirmed by DTA measurements, which reveal strong exothermic effects upon heating. The DTA curve shown in Fig. 10(b) shows at least two clearly visible exothermic effects that could be related to the transformation of the quenched-in $(\beta\text{Ti,Nb})_0$ phase and the dissolution of the metastable Ti_3Al and metastable ω' which can form during quenching and transform to ω_0 during heating.

Alloy B15 (Ti-44.7Al-12.3Nb) contains a similar amount of Nb and about 8 at.% more Al than alloy B10. Its composition lies within the two-phase field $\text{TiAl} + \omega_0$ in the entire temperature range from 700 to 900 °C (Fig. 11c and d). Alloy B12 (Ti-39.8Al-19.9Nb) with an even higher Nb content additionally contains the phase Nb_2Al . At 900 °C, the microstructure is clearly two-phase (Fig. 11b). HEXRD proves these phases to be TiAl and Nb_2Al , and the chemical compositions of the phases can be well determined by EPMA. At 800 °C, alloy B12 is three-phase $\text{TiAl} + \omega_0 + \text{Nb}_2\text{Al}$ (Fig. 11a). The HEXRD measurements of the quenched sample show the presence of a small amount of Nb_2Al (< 10 vol.%) together with the major phases TiAl and ω_0 having almost equal phase fractions. From the 800 °C diffusion couple D4-Al, a tie-line between TiAl and Nb_2Al can be determined (Table 7), which is oriented parallel to the $\text{TiAl} + \text{Nb}_2\text{Al}$ boundary of the B12 three-phase triangle. In addition, the orientation of the tie-line from alloy B15 is parallel to the $\text{TiAl} + \omega_0$ boundary of alloy B12. This is another confirmation of the existence of a three-phase equilibrium $\text{TiAl} + \omega_0 + \text{Nb}_2\text{Al}$ at 800 °C. The same three-phase equilibrium $\text{TiAl} + \omega_0 + \text{Nb}_2\text{Al}$

exists at 700 °C in alloy B12. However, the Nb_2Al phase is too small to be measured with EPMA and its phase fraction was found to be too low to be observed by the HEXRD measurements. The presence of Nb_2Al is nevertheless evident from the EPMA results, as the measured overall composition of alloy B12 at 700 °C lies above the tie-line between the measured compositions of TiAl and ω_0 . Due to its lower phase fraction compared to the 800 and 900 °C samples, its Nb content must be higher than at the higher temperatures, and, as is discussed in section 4.4, with some additional information from the literature it is possible to give at least an approximate composition.

It should be mentioned that in the two Nb-rich samples (alloys B12 and B15), small amounts of Ti_3Al were found in addition to the equilibrium phases, similar as in case of alloy B10. Most likely Ti_3Al has formed during alloy synthesis. At high temperatures (just below the solidus temperature), these alloys are single-phase $(\beta\text{Ti,Nb})$. In a detailed study of the precipitation behavior of such alloys during annealing at 800 °C, Yang et al.^[43] showed that in an initial step, metastable Ti_3Al precipitates from the $(\beta\text{Ti,Nb})$ phase instead of the equilibrium phases TiAl and ω_0 . This metastable Ti_3Al decomposes only slowly during further annealing. Therefore, we suppose that the annealing times used in the present experiments were not sufficient to completely transform the metastable Ti_3Al phase in these alloys.

A two-phase equilibrium between TiAl and Ti_3Al is observed in alloys B13 (Ti-43.4Al-4.9Nb) and B14 (Ti-45.8Al-5.9Nb) from 700 to 900 °C. As the BSE images of

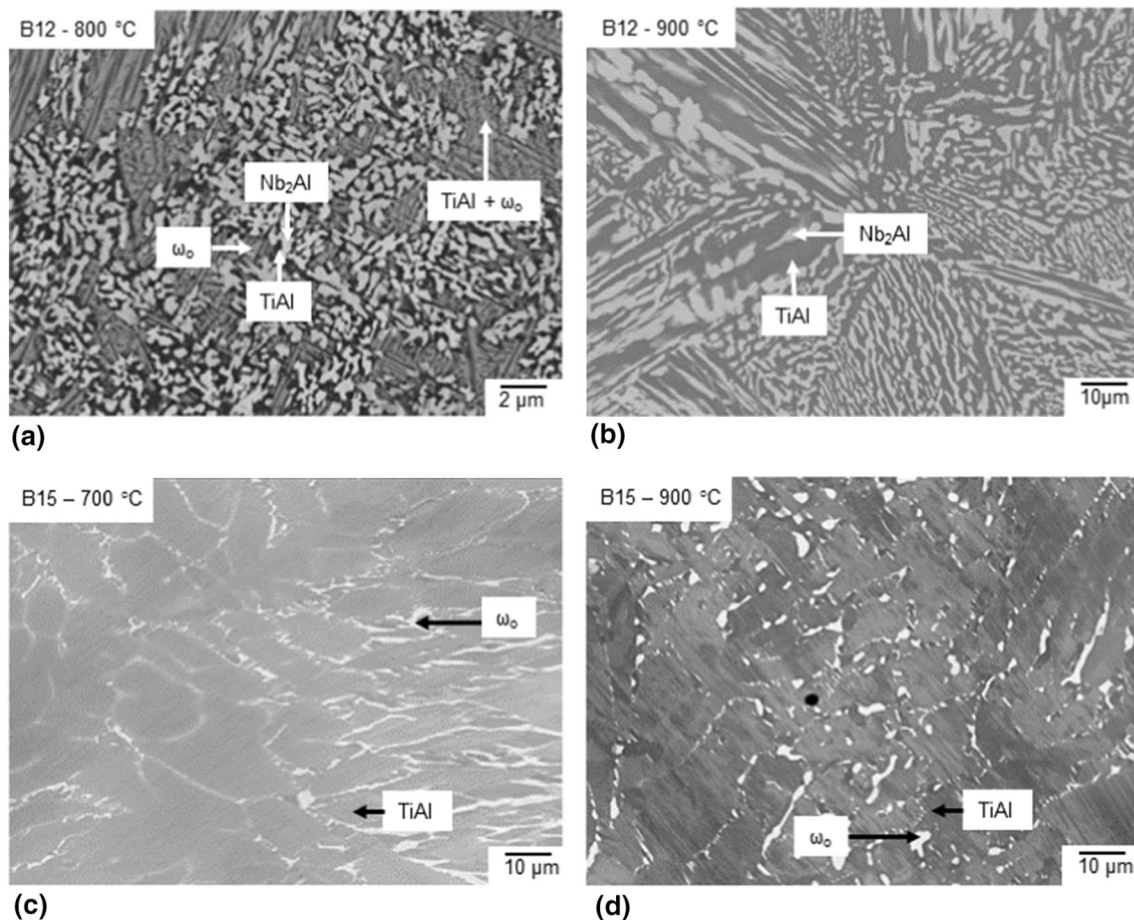


Fig. 11 BSE images of alloy B12 (Ti-39.8Al-19.9Nb) (a) heat-treated at 800 °C for 1000 h revealing the three-phase equilibrium $\text{TiAl} + \omega_0 + \text{Nb}_2\text{Al}$ and (b) heat-treated at 900 °C for 650 h showing a two-phase microstructure consisting of TiAl (dark) and Nb_2Al

(bright), and BSE images of alloy B15 (Ti-44.7Al-12.3Nb) heat-treated at (c) 700 °C/1500 h and (d) 900 °C/650 h showing a two-phase microstructure consisting of TiAl (grey) and ω_0 (bright)

alloy B13 in Fig. 12 show, parts of the samples consist of a fine lamellar microstructure, while in other areas a coarser two-phase microstructure with bright Ti_3Al in a dark TiAl matrix is observed (phases were identified with XRD measurements). In the latter areas, the phase compositions can be determined by single spot measurements. The overall composition of the fine lamellar regions is measured with a widened beam. It is found to lie close to the overall composition of the sample and exactly on the tie-line resulting from the single spot measurements confirming that the fine lamellar microstructure is also a $\text{Ti}_3\text{Al} + \text{TiAl}$ two-phase mixture. This is the case for both alloys B13 and B14 from 700 up to 900 °C. Another observation worth mentioning is that at 700 and 800 °C, the Nb content in Ti_3Al is significantly higher than in TiAl (Tables 4 and 5), which is not the case at 900 °C (Table 6). Therefore, the tie-lines at 700 and 800 °C are inclined compared to the

almost horizontal tie-line (parallel to the binary Ti–Al system) at 900 °C. This observation is consistent with the results obtained from the diffusion couples, where a similar behavior of the tie-lines is observed.

It should also be mentioned that HEXRD measurements of alloys B13 at 700 and 800 °C and B14 at 700 °C show the presence of small fractions (< 1.5 vol.%) of ω_0 phase in the samples, which are not detectable in the microstructures or in standard XRD. However, it can be excluded that ω_0 is an equilibrium phase in these alloys. If ω_0 were an equilibrium phase, the composition of both alloys would lie within the tie-triangle $\text{Ti}_3\text{Al} + \text{TiAl} + \omega_0$, which means that the compositions of Ti_3Al and TiAl in both alloys would have to be identical. This is clearly not the case. Moreover, the true three-phase equilibrium $\text{Ti}_3\text{Al} + \text{TiAl} + \omega_0$ has already been observed in the Nb-rich alloys B9 and B11 (see above and Fig. 8).

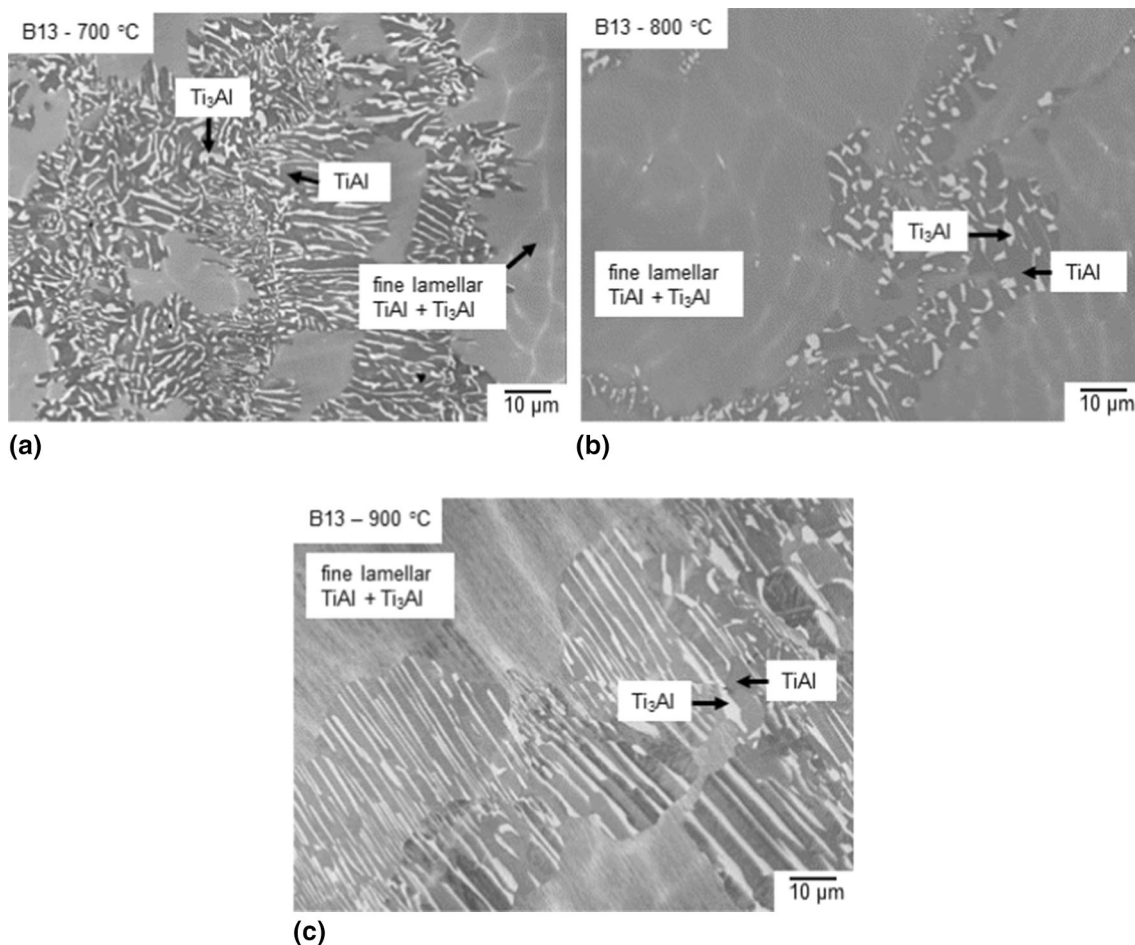


Fig. 12 BSE images of alloy B13 (Ti-43.5Al-4.9Nb) showing coarse- and fine-lamellar Ti₃Al (bright) + TiAl (dark) two-phase microstructures after heat treatment at (a) 700 °C/1500 h, (b) 800 °C/1000 h, and (c) 900 °C/650 h

4 Discussion

Based on the experimental results presented above (Tables 4, 5, 6, and 7) and some information from the literature discussed below, partial isothermal sections at 700, 800, and 900 °C were established (Fig. 14–16). For the binary boundary systems Ti–Al and Ti–Nb, the assessed phase diagrams reported in Refs. [44–46], respectively, were used. In the following, these isothermal sections are discussed in detail with special emphasis on the equilibria and homogeneity ranges of the ω_0 and O phase.

4.1 The Two-Phase Field Ti₃Al + TiAl

In the investigated temperature range between 700 and 900 °C, the two-phase field Ti₃Al + TiAl extends into the ternary system up to about 8–9 at.% Nb, as can be concluded from the results for the diffusion couples and alloys B9, B11, B13, and B14 (Fig. 13–16). Although no tie-line data were reported in the literature for this temperature

range, there are some studies on the solidification and phase transformation of alloys with compositions like B13 and B14 that confirm the existence of the two-phase region. For example, Chladil et al.^[47] investigated four alloys with a constant Al content of 45 at.% Al and Nb contents between 0 and 10 at.%. With the help of DTA and in situ HEXRD measurements, they showed that Ti₃Al and TiAl are present in alloys with up to 7.5 at.% Nb for temperatures up to above 900 °C. A similar observation was made by Rackel et al.,^[48] who found Ti₃Al and TiAl (and a small amount of 0.3 vol.% ω_0 similar as in the present experiments in alloys B13 and B14) in a sample with 45 at.% Al and 7.5 at.% Nb after homogenization at 1100 °C and heat treatment at 700 °C for 5 h with consecutive air cooling. In a recent study Dai et al.^[49] presented the results from a series of alloys with 45 at.% Al and Nb contents between 4 and 10 at.% heat-treated at 900 °C and below. Their observations at 900 °C agree with the here presented results for alloy B9, B11, B13, and B14. At 800 °C and below they found an orthorhombic phase (labeled O)

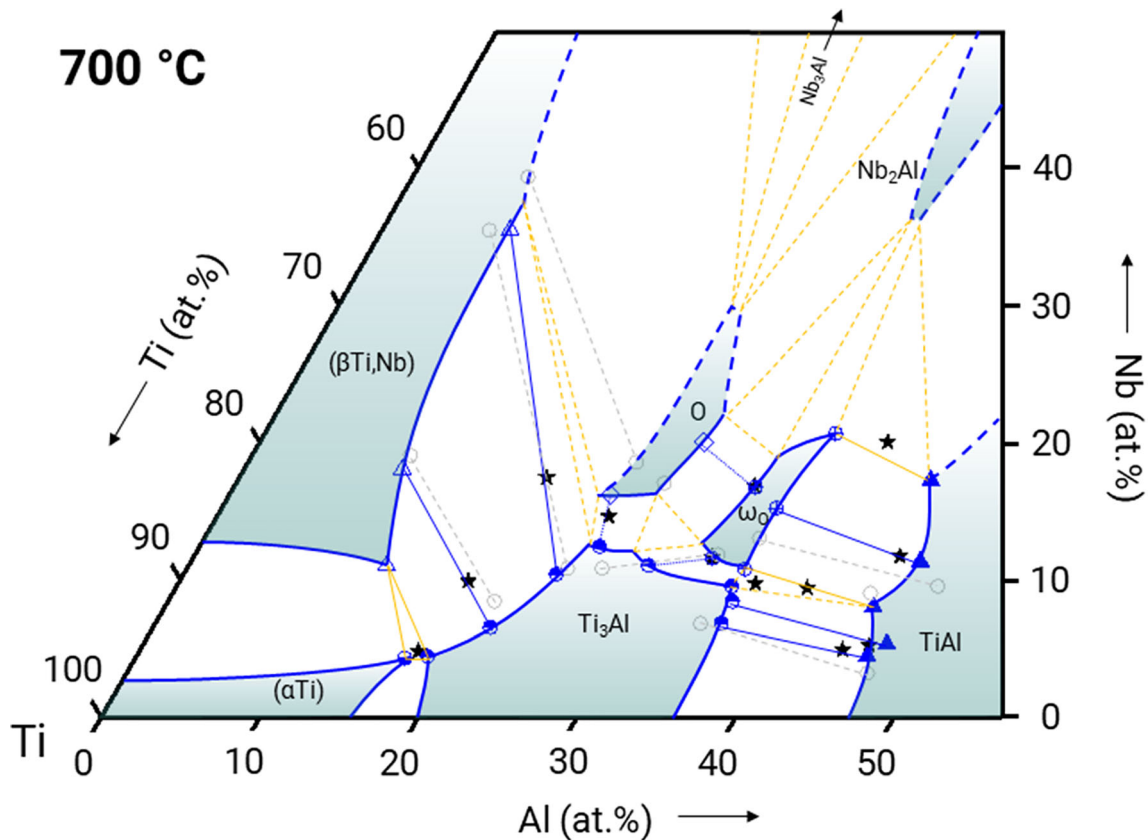


Fig. 13 Partial isothermal section of the Ti–Al–Nb system at 700 °C based on the experimental results tabulated in Tables 4 and 7. The measured overall compositions of the samples are indicated by black stars, the yellow lines mark the three-phase equilibria grey symbols

and lines indicate the data from the diffusion couples, and blue symbols and lines mark the results from bulk alloys and the resulting phase boundaries

alongside Ti_3Al and $TiAl$, which was also found by Rackel et al.^[48] in alloys with similar compositions. The phase compositions for this orthorhombic phase and Ti_3Al are consistent with the compositions measured and approximated for the Ti_3Al and ω_0 in alloys B9 and B11 (Tables 4 and 5).

At 900 °C, the $Ti_3Al + TiAl$ tie-lines of the diffusion couple D2-D1-D3 are very close to the binary Ti–Al boundary (<0.5 at.% Nb). The measured Al contents of about 36 at.% in Ti_3Al and 47 at.% in $TiAl$ (Table 7) agree very well with the phase boundaries of the $Ti_3Al + TiAl$ two-phase field in the assessed Ti–Al binary phase diagram.^[44,45] When Nb is added, the Al content in both phases remains almost constant. This results in phase boundaries almost parallel to the Ti–Nb binary system, suggesting that Nb preferentially replaces Ti in both crystal lattices. This behavior was also experimentally observed by Konitzer et al.^[50] and is predicted by density functional theory (DFT) calculations of Holec et al.^[51] for both Ti_3Al and $TiAl$. Furthermore, these results show that Nb partitions equally between Ti_3Al and $TiAl$, which is also reported in literature.^[52]

4.2 Phase Equilibria and Homogeneity Range of the ω_0 Phase

4.2.1 The Nb-Poor Limit ($Ti_3Al + TiAl + \omega_0$)

The ternary intermetallic phase ω_0 is observed as equilibrium phase in the alloys with overall Al contents from 32 to 45 at.% and Nb contents above 9 at.% (alloys B7-9, B11, B15). The three-phase equilibrium $Ti_3Al + TiAl + \omega_0$ was found in the alloys B9 (Ti-37.2Al-10.0Nb) and B11 (Ti-39.6Al-10.0Nb) between 700 and 900 °C. The tie-triangle shown in the isothermal sections at 700 and 800 °C (Fig. 13 and 14) is based on alloy B11, because some of the phase compositions of alloy B9 are only estimated values (see Tables 4 and 5). The chemical composition of the ω_0 phase in these alloys determines the lower limit of the homogeneity range of ω_0 about Nb. Within the experimental accuracy, the phase composition remains almost constant with increasing temperature and has averaged values of 10.7 at.% Nb and 34.6 at.% Al. The presence of ω_0 up to 900 °C in these two alloys agrees with the determined ω_0 -to- $(\beta Ti,Nb)_0$ transition onset temperatures

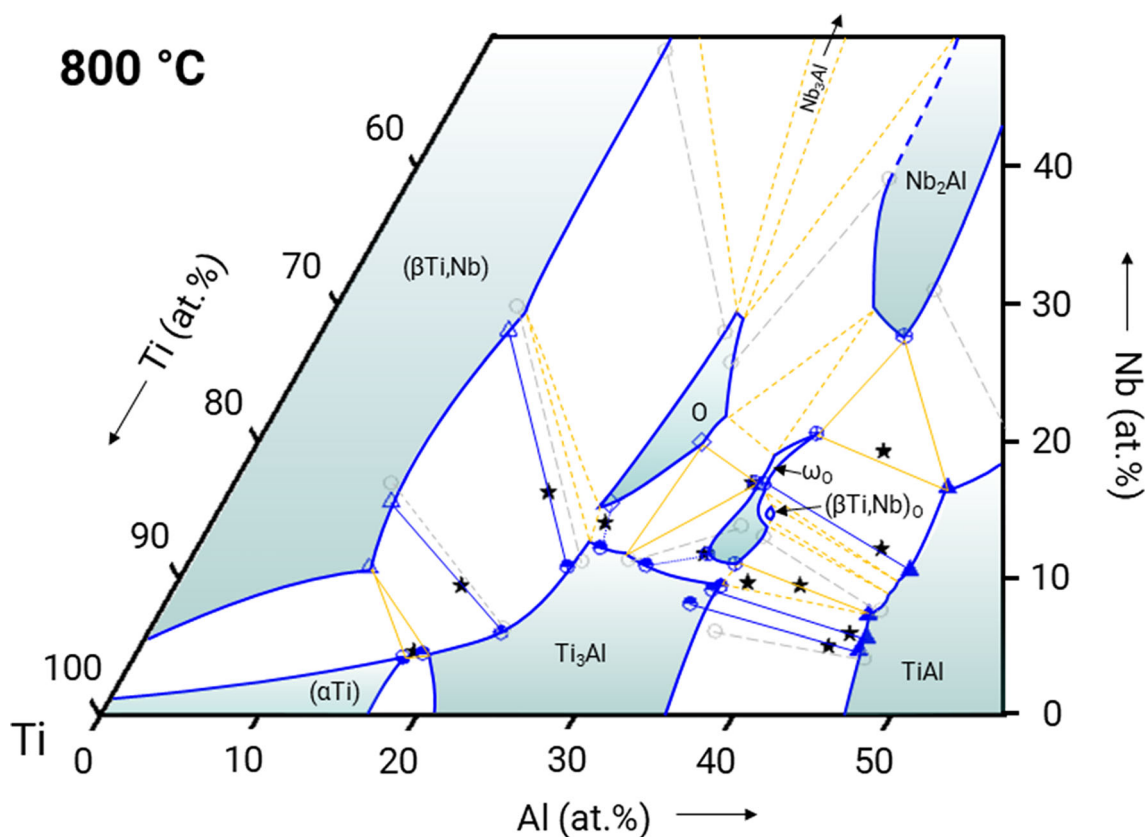


Fig. 14 Partial isothermal section of the Ti–Al–Nb system at 800 °C based on the experimental results tabulated in Tables 5 and 7 (symbols as in Fig. 13)

of 908 and 906 °C, respectively (see the corresponding alloys A4 and A3 in Ref. [8]) The existence of ω_0 in equilibrium with Ti_3Al and $TiAl$ at 900°C agrees with results reported by Xu et al.,^[22] who studied a diffusion multiple annealed at 900 °C, and Rackel et al.,^[53] who performed in situ HEXRD measurements of an alloy with the composition Ti-42Al-8.5Nb, which lies within our corresponding $Ti_3Al + TiAl + \omega_0$ tie-triangle. Yu et al.^[54] also observed the formation of ω_0 besides Ti_3Al and $TiAl$ in an alloy of the composition Ti-40Al-10Nb (like B11) after hot rolling (1150 °C) and subsequent heat treatments at 700, 800, and 900 °C. The tie-triangle $Ti_3Al + TiAl + \omega_0$ is also reported in the modelling work of Witusiewicz et al.^[35] for temperatures of 700 and 800 °C, while it is missing in their 900 °C isothermal section. They assume that the ω_0 phase exists only up to a maximum temperature of 811 °C, whereas its stability at 900 °C has been demonstrated in the present investigations and was also shown in the above-mentioned literature.^[8,22,53,54]

4.2.2 The Nb-Rich Limit ($TiAl + \omega_0 + Nb_2Al$)

The upper limit of the ω_0 homogeneity range is determined by the tie-triangle $TiAl + \omega_0 + Nb_2Al$, which is found in

alloy B12 at 700 and 800 °C. The composition of ω_0 is located at about 35.5 at.% Al and 20 at.% Nb. At 900 °C, alloy B12 consists of two-phases $TiAl$ and Nb_2Al . For this temperature, the tie-triangle can be estimated from the position of the tie-lines of the two alloys B15 ($TiAl + \omega_0$) and B12 ($TiAl + Nb_2Al$) (Fig. 15). Since their compositions for $TiAl$ are close to each other, the $TiAl$ corner of the tie-triangle must be very near to this point. And since, for thermodynamic reasons, tie-lines which are very near to the sides of a tie-triangle can be expected to be (almost) parallel to the tie-triangle, the compositions of Nb_2Al and ω_0 are supposed to lie close to the corresponding compositions in alloy B12 and B15 (Fig. 15). This results in a decrease of about 2 at.% for the maximum Nb content of ω_0 between 800 °C (20.6 at.%) and 900 °C (~ 18.0 at.%), while the Al content remains almost constant being ~34.5 at.% at 900 °C. No information is available from the literature about this tie-triangle at 700 and 800 °C. For 900 °C, the diffusion multiple experiment of Xu et al.^[22] confirms the existence of the $TiAl + \omega_0 + Nb_2Al$ three-phase field. Since they assumed an only small, nearly circular ω_0 phase field (for a discussion of this aspect, see also section 4.2.6), they give a much lower value for the Nb content (15 at.%),

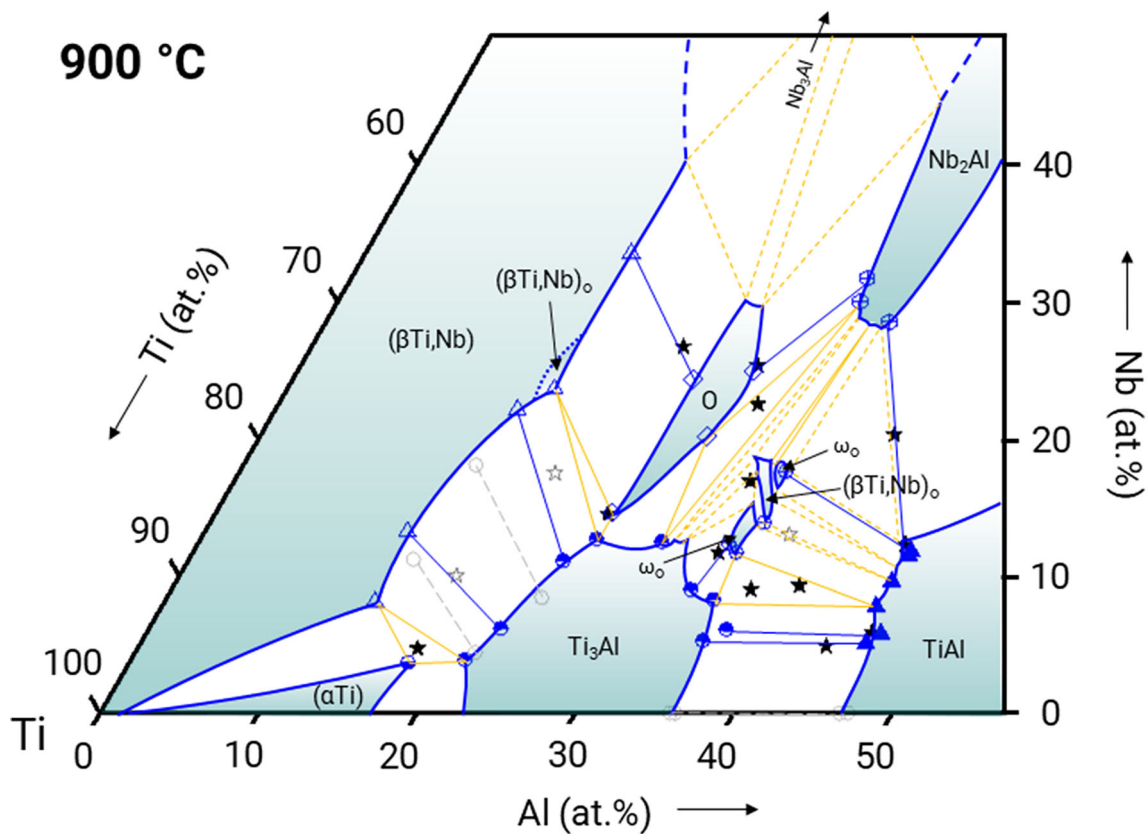


Fig. 15 Partial isothermal section of the Ti–Al–Nb system at 900 °C based on the experimental results tabulated in Tables 6 and 7 (symbols as in Fig. 13, unfilled stars: nominal alloy composition)

while the Al content (34.5 at.%) is identical to the value estimated here.

4.2.3 Equilibria on the Al-Rich Side—Formation of the $(\beta\text{Ti,Nb})_0$ Phase from ω_0

The two-phase equilibrium $\text{TiAl} + \omega_0$ is observed in alloy B15 at 700 to 900 °C and is also found in the diffusion couples heat-treated at 700 and 800 °C. It is worth to mention that the Al contents here on the Al-rich side of the ω_0 phase field range from 33.5 to 35.4 at.% (and do not include the stoichiometric value of 37.5 at.% corresponding to the commonly used formula “ Ti_4NbAl_3 ”; see section 4.2.6 for a discussion of this aspect). Bendersky et al.^[15] investigated an alloy of composition Ti-37.5Al-12.5Nb lying in this two-phase field. After homogenization for 4 h at 1400 °C in the $(\beta\text{Ti,Nb})_0$ single-phase state, their sample was annealed at 700 °C for 624 h. In agreement with the present findings, they observed an equilibrium between the ω_0 phase and TiAl. Their measured phase compositions (Ti-34.5Al-13Nb for ω_0 and Ti-50Al-9Nb for TiAl) are very similar to those determined in our 700 °C diffusion couple (Ti-35Al-13Nb for ω_0 and Ti-48Al-9.5Nb for TiAl).

Interestingly, in addition to the two equilibrium phases ω_0 and TiAl, Bendersky et al.^[15] found a trace amount of Ti_3Al , similar as in our experiments on alloys B12 and B15. As already mentioned in section 3 and described in detail in Ref. [43] for a Ti-40Al-8Nb alloy, this could result from the easy formation of metastable Ti_3Al and its slow transformation to the ω_0 equilibrium phase. The slow formation process of the ω_0 phase from Ti_3Al was also described by Song et al.,^[55] who performed TEM studies of the structural relation between Ti_3Al and ω_0 in a Ti-45Al-9Nb alloy annealed at 850 °C. Another possible explanation for the presence of non-equilibrium Ti_3Al phase is the effect of interstitial impurity elements. High amounts of such interstitial elements (which are not observed in our experiments) tend to shift phase compositions of phase equilibria with hexagonal phases, such as Ti_3Al , to higher Nb contents.^[56]

As for the formation/dissolution temperature of the $(\beta\text{Ti,Nb})_0$ phase in the ternary system, the only information available from literature comes from in situ neutron diffraction experiments on a Ti-36.5Al-12.9Nb alloy in the temperature range between 700 and 960 °C.^[21] In this work, the transformation from ω_0 to $(\beta\text{Ti,Nb})_0$ was found

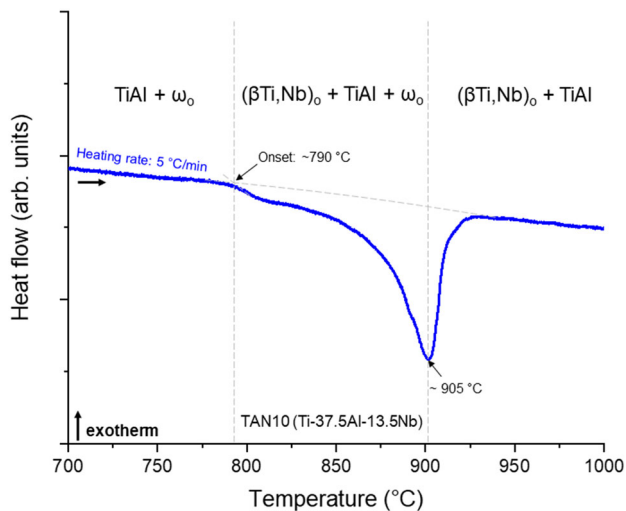


Fig. 16 DTA heat flow curve of alloy B10 (heat-treated at 1000 °C for 400 h, heating rate 5 °C/min) showing the ω_0 -to- $(\beta\text{Ti,Nb})_0$ transformation

to start at about 800 °C. The composition of our alloy B10 (Ti-37.0Al-13.5Nb) is very similar to the one studied by neutron diffraction. In DTA measurements of this alloy, the onset of a reaction is visible at about 790 °C (Fig. 16). Therefore, from the observations of Sadi et al.^[21] together with the presence of the thermal effect in the DTA measurement, we conclude that in alloy B10 the $(\beta\text{Ti,Nb})_0$ phase starts to form at ~ 790 °C from the two phases TiAl and ω_0 . Therefore, the temperature of the eutectoid reaction $(\beta\text{Ti,Nb})_0 \rightleftharpoons \text{TiAl} + \omega_0$ must be lower than measured in alloy B10. The composition of the $(\beta\text{Ti,Nb})_0$ phase at 800 °C in the alloy used for the neutron diffraction experiments was reported to be Ti-34.5Al-15.1Nb,^[20] and this value was used in our 800 °C isothermal section for drawing the $(\beta\text{Ti,Nb})_0$ phase field (Fig. 14). From the DTA curve in Fig. 16, the transformation of ω_0 to $(\beta\text{Ti,Nb})_0$ in our alloy B10 is finished at ~ 905 °C, which corresponds to the peak temperature. XRD of this alloy after heat treatment at 900 °C confirms the coexistence of $(\beta\text{Ti,Nb})_0$, ω_0 , and TiAl (Fig. 10). The composition of the $(\beta\text{Ti,Nb})_0$ phase measured in alloy B10 at 900 °C (Ti-35.0Al-13.9Nb) marks the Nb-lean end of the small phase field. The tie-triangle at this temperature is already very narrow (Fig. 15) as the sample becomes two-phase $(\beta\text{Ti,Nb})_0 + \text{TiAl}$ at ~ 905 °C (Fig. 16).

4.2.4 Equilibria on the Ti-Nb-Rich Side

The Ti-rich phase boundary of the ω_0 phase field at low Nb contents is determined by the two-phase equilibria between Ti_3Al and ω_0 in alloy B7 (Ti-32.8Al-12.2Nb) between 700 and 900 °C (Fig. 7a). The same phase equilibrium with very similar microstructures was observed by Song et al.^[57]

in an alloy with nominal composition Ti-34Al-13Nb after annealing for 100 h at 700 and 900 °C (cf. Fig. 8 in section 3 and Fig. 3 in Ref. [57]). The compositions in Ref. [57] were measured by TEM-EDS and are slightly different from the present values. Regarding the accuracy of their composition values from TEM-EDS, Song et al. point out that “Although the EDS analysis on TEM cannot be as precise as that obtained on electron microprobe, it still reflects the composition redistribution between different phases.”^[57] Thus, the results can be taken as a confirmation of our data regarding the existence and position of the $\text{Ti}_3\text{Al} + \omega_0$ two-phase field.

At 700 and 800 °C, the ω_0 phase field is further defined by the adjacent tie-triangle $\text{Ti}_3\text{Al} + \text{O} + \omega_0$, which is observed at 800 °C in alloy B8 (Ti-32.4Al-17.3Nb) both in the quenched microstructure as well as by in situ HEXRD measurements. At 700 °C (Fig. 7c), the same alloy is two-phase $\text{O} + \omega_0$, indicating that the position of the $\text{Ti}_3\text{Al} + \text{O} + \omega_0$ tie-triangle (or at least the $\text{O} + \omega_0$ tie-line of the triangle) must have shifted to lower Nb contents. The existence of this three-phase equilibrium is confirmed by results of Sadi^[20] in a Ti-29.5Al-14.2Nb alloy heat-treated at 700 °C. As the exact phase compositions at 700 °C are not known, we tentatively estimated the position of the tie-triangle based on the measured nearby tie-lines (see Fig. 13).

The existence of the two-phase equilibrium $\text{O} + \omega_0$, which was observed at 700 °C in alloy B8, was also confirmed by Bendersky et al.,^[58] who performed TEM studies on a Ti-30Al-20Nb alloy but did not determine the phase compositions. On the Nb-rich side of this two-phase field, the tie-triangle $\text{O} + \omega_0 + \text{Nb}_2\text{Al}$ is located. The existence of this three-phase equilibrium at 700 °C was confirmed by Sadi.^[20] From the present investigations, no experimental data are available in this composition range at 700 and 800 °C.

At 900 °C (Fig. 7d), the phase equilibria in this composition range between the phases Ti_3Al , O , ω_0 , and Nb_2Al differ significantly from the lower temperatures. This is a result of the appearance of the $(\beta\text{Ti,Nb})_0$ phase and the onset of decomposition of the ω_0 phase, which leads to a splitting of the ω_0 phase field as discussed in the next section.

4.2.5 Splitting of the ω_0 Phase Field

As reported above in section 4.2.1 and 4.2.2 and visible in Fig. 13–15, the ω_0 phase exhibits an extended homogeneity range from about 10 to 20 at.% Nb. DTA investigations on a series of ternary alloys containing the ω_0 phase have revealed that the onset temperature of the decomposition reaction depends in an unexpected way on the composition.^[8] The highest stability, i.e., the highest onset

temperatures of the decomposition reaction were found for ω_o compositions at the Nb-poor and Nb-rich end ($T_{\text{onset}} \sim 920$ °C) of the homogeneity range, while at intermediate Nb contents there is a stability minimum ($T_{\text{onset}} < 900$ °C). In the case of alloy B8 (corresponding to alloy A8 in Ref. [8]), ω_o starts to transform to $(\beta\text{Ti,Nb})_o$ at 897 °C (Fig. 17),

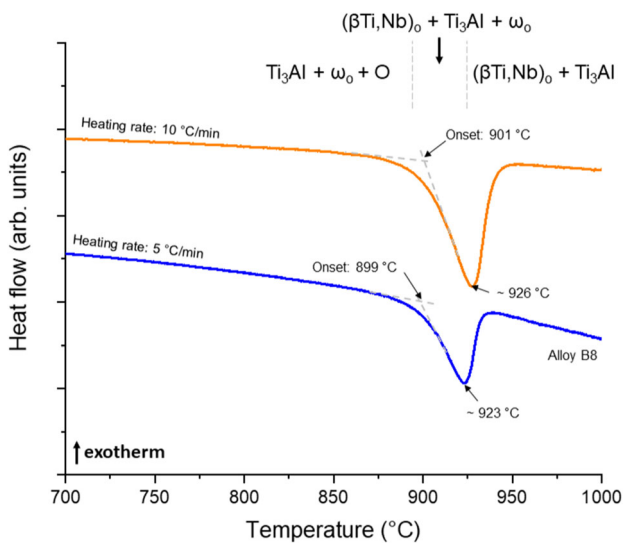


Fig. 17 DTA heat flow curve of alloy B8 (heat-treated at 700 °C for 1500 h, heating rate 10 and 5 °C/min) showing the heating rate dependent onset temperature of the ω_o -to- $(\beta\text{Ti,Nb})_o$ transformation. The onset temperature is heating rate dependent and has been determined in Ref. [8] to be 897 °C

which means that above this temperature (i.e. specifically in the isothermal section at 900 °C), the $(\beta\text{Ti,Nb})_o$ phase must be present on the Al-poor side of the ω_o phase field, and the overall composition of alloy B8 must be located in a tie-triangle/two-phase field that includes $(\beta\text{Ti,Nb})_o$.

One possible way to achieve this is that the $(\beta\text{Ti,Nb})_o$ phase field formed below 790 °C on the Al-rich side of the ω_o phase field further constricts the ω_o phase field with increasing temperature and finally splits it into two separate phase fields (at an unknown temperature between 800 and 897 °C, therefore the temperature is estimated to be 850 ± 45 °C). This would lead to the formation of two new tie-triangles $(\beta\text{Ti,Nb})_o + \text{O} + \omega_o$ (violet filled tie-triangles in Fig. 18a) in the former $\text{O} + \omega_o$ two-phase field. The lower of these two tie-triangles must take part in a transition-type reaction with the $\text{Ti}_3\text{Al} + \text{O} + \omega_o$ three-phase equilibrium ($(\beta\text{Ti,Nb})_o + \text{Ti}_3\text{Al} \rightleftharpoons \text{O} + \omega_o$). Similar reactions have to occur between the upper $(\beta\text{Ti,Nb})_o + \text{O} + \omega_o$ and $\text{O} + \omega_o + \text{Nb}_2\text{Al}$ tie-triangles ($(\beta\text{Ti,Nb})_o + \text{Nb}_2\text{Al} \rightleftharpoons \text{O} + \omega_o$). This leads to four new tie-triangles $(\beta\text{Ti,Nb})_o + \omega_o + \text{Ti}_3\text{Al}/\text{Nb}_2\text{Al}$ and $(\beta\text{Ti,Nb})_o + \text{O} + \text{Ti}_3\text{Al}/\text{Nb}_2\text{Al}$ as shown in Fig. 18(b) (green-shaded tie-triangles). The two three-phase equilibria containing ω_o will take part in the dissolution of the remaining ω_o above 900 °C, and the tie-triangles containing the O phase must undergo another transition-type reaction ($\text{Ti}_3\text{Al} + \text{Nb}_2\text{Al} \rightleftharpoons (\beta\text{Ti,Nb})_o + \text{O}$) to result in the phase equilibria that are observed at 900 °C (Fig. 15). The described transition-type reactions must take place between 897 and 900 °C. Alloy B8 would be only involved in the transition reaction $(\beta\text{Ti,Nb})_o +$

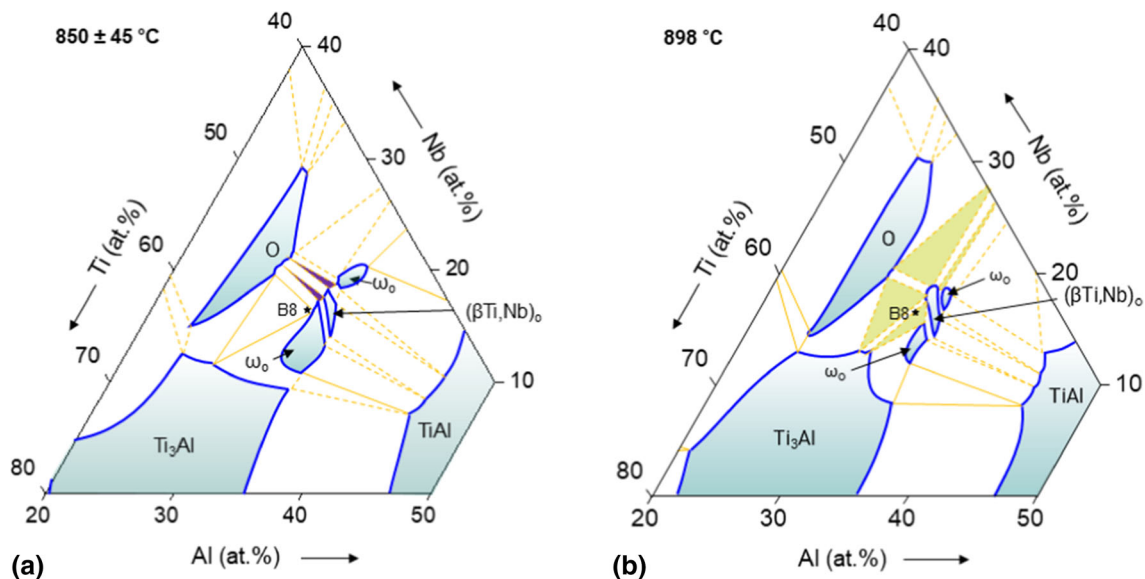


Fig. 18 Schematic partial isothermal sections (a) at 850 ± 45 °C just above the (unknown) temperature where the growing $(\beta\text{Ti,Nb})_o$ phase has split the ω_o phase field into two parts resulting in the two new

ternary triangles marked in violet, and (b) at 898 °C after the transition-type reaction $(\beta\text{Ti,Nb})_o + \text{Ti}_3\text{Al} \rightleftharpoons \text{O} + \omega_o$ on the Nb-poor and $(\beta\text{Ti,Nb})_o + \text{Nb}_2\text{Al} \rightleftharpoons \text{O} + \omega_o$ on the Nb-rich side

$\text{Ti}_3\text{Al} \rightleftharpoons \text{O} + \omega_o$ at 897 °C changing its three-phase equilibrium from $\text{Ti}_3\text{Al} + \text{O} + \omega_o$ to $(\beta\text{Ti,Nb})_o + \text{Ti}_3\text{Al} + \omega_o$. Therefore, a slight temperature deviation of the heat treatment furnace by, e.g., 5 °C (i.e., 895 °C instead of the intended value of 900 °C) would be sufficient to explain the observed $\text{Ti}_3\text{Al} + \text{O} + \omega_o$ equilibrium in alloy B8 (Fig. 7(d)). On further heating of alloy B8, the transformation of the ω_o phase to $(\beta\text{Ti,Nb})_o$ continues until the sample enters the two-phase field $\text{Ti}_3\text{Al} + \text{O}$, which happens at approximately 915 °C (which is a rough estimation from an extrapolation of peak temperatures from DTA heating curves to heating rate 0 °C/min). At 1000 °C, the alloy is still in this two-phase field as was confirmed by a heat-treated sample and is reported in Part II of this study.^[36]

4.2.6 Stoichiometry of the ω_o Phase—Revised Formula

In the literature, the formula Ti_4NbAl_3 is commonly used for the ω_o phase, which corresponds to a stoichiometric composition of Ti-37.5Al-12.5Nb. The present investigations show that the homogeneity range of ω_o between 700 and 900 °C extends parallel to the Ti-Nb axis along an almost constant Al content varying only slightly between 32.5 and 36 at.%. In agreement with that, Xu et al.^[22] found equilibrium compositions of the ω_o phase at 900 °C in the range between 33.1 and 34.5 at.% Al. Obviously, the composition corresponding to the formula is outside of the homogeneity range of the ω_o phase. The formula Ti_4NbAl_3 stems from the fundamental work of Bendersky et al.,^[15] who were the first to describe the transformation from the ordered $(\beta\text{Ti,Nb})_o$ phase and the structure of the ω_o phase in detail. Reading their original work,^[15] it becomes clear that there was a misunderstanding in the later literature that led to the wrong phase designation. In their paper, Bendersky et al.^[15] never referred to the equilibrium ω_o phase by this formula, but instead Ti_4NbAl_3 corresponds to the alloy composition they studied. This alloy was found to be single-phase $(\beta\text{Ti,Nb})_o$ after annealing at 1400 °C, and after quenching to room temperature it transformed to a metastable single-phase ω'' structure with a trigonal unit cell and space group $P\bar{3}m1$. This displacive transformation from B2-ordered $(\beta\text{Ti,Nb})_o$ to the metastable, trigonal ω'' structure occurs without any change in chemistry and the trigonal ω'' can be described by the formula Ti_4NbAl_3 (or $\text{Ti}_3\text{Al}_{2.25}\text{Nb}_{0.75}$ as used by Shoemaker et al.^[59]). However, the final transformation to the equilibrium ω_o phase, which was observed by Bendersky et al.^[15] to occur after prolonged annealing at 700 °C, is “strongly first order” and does not only affect the crystal structure but also involves a change of chemical composition accompanied by the precipitation of a second phase, which is TiAl. Thus, the transformation sequence to reach the equilibrium state is

$(\beta\text{Ti,Nb})_o \rightarrow \omega'' \rightarrow \text{TiAl} + \omega_o$. Since TiAl is richer in Al compared to the alloy composition (37.5Al), it is obvious that the equilibrium ω_o phase must contain a lower amount of Al relative to the alloy composition. In case of their Ti-37.5Al-12.5Nb alloy, Bendersky et al.^[15] obtained a composition of Ti-34.5Al-13Nb for their ω_o phase (Table 3 in Ref. [15]), which is in perfect agreement with our 700 °C isothermal section (Fig. 13).

Interestingly, the crystal structure of the ω_o phase is of the $B8_2$ type, prototype Ni_2In , and Pearson symbol $hP6$. Regarding this structure type and the observed homogeneity range of about 10 to 20 at.% Nb and 32.5 to 36 at.% Al, a formula of the type $(\text{Ti,Nb})_2\text{Al}$ would be a more appropriate for the ω_o phase. With Al located on the In site and Ti and Nb sharing the Ni site of the prototype structure, this corresponds to a stoichiometric Al content of 33.3 at.%. The unit cell of the $B8_2$ crystal structure contains three independent Wyckoff sites ($2a$), ($2c$), and ($2d$), where – in case of the prototype phase Ni_2In – the In atoms occupy the ($2c$) positions and Ni the two other sites. For a ternary phase such as the ω_o phase, the existence of the three Wyckoff sites offers the additional possibility of a non-statistical site occupation of Nb (respectively Ti) on the two sites ($2a$) and ($2d$). Structure refinements of single-crystal XRD data by Bendersky et al.^[15] indicate that the Nb atoms prefer the ($2a$) sites (i.e., Ti occupies all the ($2d$) sites and the remaining ($2a$) sites).

Thus, we suggest using the more appropriate designation $(\text{Ti,Nb})_2\text{Al}$ for the ω_o phase. The range of Nb contents then can be described approximately by $(\text{Ti}_{1-x}\text{Nb}_x)_2\text{Al}$ with $0.15 < x < 0.3$.

4.3 Phase Equilibria and Homogeneity Range of the O Phase

The above-described reaction sequence, which resulted from the splitting of the ω_o phase, also influences the Al-rich side of the homogeneity range of the neighboring O phase, which is the second ternary intermetallic phase of the system and has a stoichiometric composition of Ti-25Al-25Nb. As mentioned above, the presence of the two tie-triangles $\text{Ti}_3\text{Al} + \text{O} + \omega_o$ and $\text{O} + \omega_o + \text{Nb}_2\text{Al}$ as well as the two-phase field $\text{O} + \omega_o$ are well documented at 700 and 800 °C. The same two tie-triangles were found by Xu et al.^[22] in their diffusion multiple studies at 900 °C. However, the present investigations reveal that at 900 °C, the $\text{O} + \omega_o$ two-phase field no longer exists and instead the O phase is in a three-phase equilibrium with Ti_3Al and Nb_2Al . This three-phase equilibrium was observed in one part of alloy B6 (overall composition Ti-30.3Al-22.5Nb) as described above (see also Fig. 7 and 15). The same tie-triangle $\text{Ti}_3\text{Al} + \text{O} + \text{Nb}_2\text{Al}$ was also reported by Sadi^[20] at 900 °C (and 800 °C).

Similar as in the case of the ω_0 phase, the homogeneity range of the O phase mainly extends parallel to the Ti-Nb axis. The maximum Nb content in the O phase is determined by its equilibria with Nb_3Al , which, however, did not occur in the alloys studied here. Xu et al.^[22] report a maximum value of 26.7 at.% Nb for the O phase. However, the results of our diffusion couple D4-Al, which was heat-treated at 800 °C, indicate that the maximum Nb content in the O phase must be higher and amounts to about 30 at.%. This is also consistent with results from Kestner-Weykamp et al.,^[28] who found that an alloy of composition Ti-25Al-30Nb was single-phase O phase at 800 °C and agrees with the work of Rowe et al.,^[18] who reported an upper limit of the O phase field of 30 at.% Nb.

The Nb-poor boundary of the O phase field is defined by the two-phase field between Ti_3Al and O. From alloy B4, we find minimum Nb contents of 16.2, 15.5, and 14.6 at.% at 700, 800, and 900 °C, respectively. Xu et al.^[22] again report a different value of 19.3 at.% Nb at 900 °C, while our data are in good agreement with the work of Kestner-Weykamp et al.^[28] and Rowe et al.^[18] (who give a minimum value of 15 at.% Nb for 900 °C).

The tie-triangle $(\beta\text{Ti,Nb})_0 + \text{Ti}_3\text{Al} + \text{O}$ is observed in alloy B4 at 900 °C. In alloys with similar composition, Rowe et al.^[18] (Ti-25.2Al-15.7Nb) and Kamat et al.^[60] (Ti-24.0Al-15.0Nb and Ti-24.0Al-20.0Nb) also observed this three-phase equilibrium after heat treatment at 900 °C. However, they did not analyse the phase compositions and especially the data of Kamat et al.^[60] suggests a very small stability range of the O phase which could not be confirmed by other investigations. This might be a result of the thermomechanical heat treatment of the alloys and the fact that the actual composition of the alloy was never measured. At 700 and 800 °C, none of the present alloys contained this three-phase equilibrium, but the position of its tie triangle could be estimated from the two-phase alloys B3 and B4 and the diffusion couples.

On the Al-poor side of the O phase, there is an extended two-phase field with the $(\beta\text{Ti,Nb})$ solid solution. Alloys in this composition range have been studied by various authors as new structural materials with even better mechanical properties than the TiAl-based alloys, see, e.g., the review of Zhang et al.^[9] However, these studies focus on mechanical properties and microstructural aspects of such alloys and no data on equilibrium phase compositions were reported. At 900 °C, many of the alloys studied by Rowe et al.^[18] lie in this phase field and they concluded that the Al-poor phase boundary of the O phase field is at a constant Al content of about 25 at.%. Xu et al.^[22] report a similar value of 25.2 at.% Al. This value agrees with our results for alloys B4 and B5 at 900 °C (25.0 and 25.3 at.% Al, respectively). At 700 and 800 °C, we found the two-phase equilibrium $(\beta\text{Ti,Nb}) + \text{O}$ in the diffusion couples

D3-Al (700 °C) and D4-Al (800 °C) giving Al contents for the O phase of 25.0 and 25.5 at.%, respectively (Table 7). As is visible from the isothermal sections, the minimum Al content most likely is reached at the lower, Nb-poor end of the phase field and is tentatively estimated as ~ 24 at.%. It should also be mentioned that the $(\beta\text{Ti,Nb})$ phase at 700 and 800 °C is disordered for all compositions. At 900 °C, B2-ordering only occurs in a small composition range corresponding to the highest Al contents and is observed in alloy B4, while alloys B1-3 and B5 contain disordered $(\beta\text{Ti,Nb})$ phase, see Fig. 15.

The maximum Al contents found in the O phase are in the range between 28 and 30 at.% Al. This is in agreement with the results of Xu et al.,^[22] who reported a maximum Al content of 28.2 at.% for this phase at 900 °C. Furthermore, Rowe et al.^[18] also gave 28 at.% as the upper Al limit for the composition range of the O phase at 900 °C. There is no information from the literature about lower temperatures, but the present data indicate a slight decrease of the maximum Al content with decreasing temperature.

By taking all data into account, the homogeneity range of the O phase is well determined in the temperature range 700-900 °C. The Nb-rich end of its homogeneity range is located at about 30 at.% Nb for all temperatures and the Nb-poor limit lies at about 15 at.%. As for the Al contents, the maximum extension of the O phase field ranges from about 24 to 28 at.%.

4.4 Solubility of Ternary Elements in the Boundary Phases (αTi) , $(\beta\text{Ti,Nb})$, Ti_3Al , and Nb_2Al

The solubility of Nb in the (αTi) solid solution slightly increases with increasing the Al content and reaches its maximum value in the three-phase equilibrium with Ti_3Al and $(\beta\text{Ti,Nb})$ (alloy B1). Within the accuracy of our experiments, this value is independent of temperature and amounts to an averaged value of (4.0 ± 0.5) at.% Nb. The associated Al contents also vary only slightly and are in the range between 17.0 and 17.6 at.%. Xu et al.^[22] extracted a similarly low value of 3.3 at.% for the solubility of Nb (at an Al content of 15.6 at.%) from their diffusion couple experiments at 900 °C.

Ti_3Al has a significantly higher solubility for Nb. From the present data, a solubility of (12.5 ± 0.5) at.% Nb can be estimated for an Al content of (25 ± 0.5) at.%. Temperature again has only a very weak effect on the Nb solubility (increasing from about 12.4 at.% at 700 °C to 12.8 at.% at 900 °C). Xu et al.^[22] found a higher value of 16 at.% Nb at 900 °C, whereas our results are in good agreement with those of Sadi,^[20] who measured maximum Nb contents in Ti_3Al of 13.2, 11.8, and 12.8 at.% Nb at 700, 800, and 900 °C, respectively.

In the (β Ti,Nb) solid solution, considerable amounts of Al are soluble throughout the investigated Nb-Ti composition range. With increasing temperature, the (β Ti,Nb) phase field grows continuously into the ternary system, which can already be seen, for example, in the increasing Al content of (β Ti,Nb) in alloys B2 and B3 between 700 and 900 °C (Tables 4–6). A comparison of the isothermal sections in Fig. 13–15 shows that for example along a constant Nb content of 25 at.% the extension of the (β Ti,Nb) phase increases from about 8 to 12 and finally to 17 at.% Al at 700, 800, and 900 °C, respectively. Experimental data from literature are in the same range. Xu et al.^[22] obtained a maximum Al content of 14.7 at.% in their experiments at 900 °C, Rowe et al.^[18] estimated a solubility of 13–15 at.% Al, and in Sadi's work^[20] values of 14.3, 14.6, and 16.0 at.% Al are reported for 700, 800, and 900 °C, respectively.

Nb₂Al is the binary phase with the highest ternary solubility in the Ti–Al–Nb system. The maximum Ti contents in the temperature range 700–900 °C exceed 30 at.%. Our data indicate a solubility of about 37.5 at.% at 900 °C (in good agreement with a value of 37.1 at.% reported by Xu et al.^[22]) and 36 at.% at 800 °C. For 700 °C, the present data indicate a further, possibly even stronger decrease in solubility. However, no value could be measured in the present experiments for this temperature. Even though the presence of Nb₂Al in alloy B12 is evident from EPMA grid measurements, the precipitates were too small to be measured with EPMA. The non-visibility of Nb₂Al peaks in HEXRD of this sample reveals that the phase fraction is very low. This means the Nb₂Al corner of the respective tie-triangle must be far away from the overall composition, which is the case if the Ti content is further decreased. This is also in accordance with the calculated phase diagram of Witusiewicz et al.^[35] From their isothermal sections, approximate values for the Ti solubility of 37, 36, and 30 at.% can be read for 900, 800, and 700 °C, respectively. As the values for 900 and 800 °C agree very well with our results, we adopted their value for 700 °C for a tentative drawing of the 700 °C isothermal section in this range.

5 Conclusions

Three partial isothermal sections of the Ti–Al–Nb system at 700, 800, and 900 °C were constructed covering the composition range 0–50 at.% Al and 0–50 at.% Nb. For this purpose, a systematic study of a series of heat-treated ternary Ti–Al–Nb alloys and several solid–solid and liquid–solid diffusion couples was performed by EPMA, (HE)XRD, TEM, and DTA.

The two intermetallic compounds ω_o and O were found to be stable up to above 900 °C and exhibit extended composition ranges.

The O phase extends parallel to the Ti–Nb axis between 15 and about 30 at.% Nb along an only slightly varying Al content of 24–28 at.%.

The phase field of ω_o also extends along an approximately constant Al content. In this case, the Nb content covers a range from 10 to 20 at.% and the Al content varies between 32.5 and 36 at.%.

The homogeneity range of the ω_o phase does not include the composition Ti₄NbAl₃ but can instead be well described by a formula (Ti,Nb)₂Al. This new formula fits exactly to the well-established crystal structure type (prototype Ni₂In, *hP6*) of the ω_o phase and is suggested to replace the old phase designation Ti₄NbAl₃.

With increasing temperature, the phase field of ω_o becomes more and more constricted. This is related to the growing phase field of the (β Ti,Nb)_o phase, which forms as a result of a eutectoid-type reaction at 790 °C from TiAl and ω_o phase. At 900 °C, the phase field of ω_o is split into two parts by the (β Ti,Nb)_o field. Based on DTA measurements and the observed phase equilibria, a reaction sequence is suggested that describes the splitting of the phase field and the evolution of the resulting phase equilibria.

The solubility of Nb in the (α Ti) solid solution and in Ti₃Al is nearly constant in the investigated temperature range 700–900 °C. It amounts to (4.0 ± 0.5) at.% Nb (Al content 17.0–17.6 at.%) for (α Ti) and to (12.5 ± 0.2) at.% Nb (Al content 24.9–25.5 at.%) in case of Ti₃Al. For the solubility of Al in the (β Ti,Nb) solid solution, values of about 12 at.% were measured at 700 and 800 °C, while this value increases up to about 17 at.% at 900 °C. Nb₂Al extends far into the ternary system. The solubility of Ti reaches about 37 at.% at 900 °C and decreases to about 35 at.% at 800 °C.

Within the extended phase field of the disordered (β Ti,Nb) solid solution, B2-ordering occurs at 900 °C in a small composition range at the Al-rich boundary at about 16 at.% Al and Nb contents near 25 at.%. At 700 and 800 °C, no B2-ordering occurs because of the lower Al solubility.

Further isothermal sections for temperatures of 1000 to 1300 °C were investigated and will be presented in a forthcoming Part II paper.

Supplementary Information The online version contains supplementary material available at <https://doi.org/10.1007/s11669-022-00963-8>.

Acknowledgment The authors gratefully acknowledge funding from the Clean Sky 2 Joint Undertaking under the European Union's

Horizon 2020 research and innovation program under grant agreement No. 820647.

Open Access This article is licensed under a Creative Commons Attribution 4.0 International License, which permits use, sharing, adaptation, distribution and reproduction in any medium or format, as long as you give appropriate credit to the original author(s) and the source, provide a link to the Creative Commons licence, and indicate if changes were made. The images or other third party material in this article are included in the article's Creative Commons licence, unless indicated otherwise in a credit line to the material. If material is not included in the article's Creative Commons licence and your intended use is not permitted by statutory regulation or exceeds the permitted use, you will need to obtain permission directly from the copyright holder. To view a copy of this licence, visit <http://creativecommons.org/licenses/by/4.0/>.

Funding Open Access funding enabled and organized by Projekt DEAL.

References

1. H. Clemens and S. Mayer, Design, Processing, Microstructure, Properties, and Applications of Advanced Intermetallic TiAl Alloys, *Adv. Eng. Mater.*, 2013, **15**(4), p 191-215. <https://doi.org/10.1002/adem.201200231>
2. S.A. Raji, A.P.I. Popoola, S.L. Pityana, and O.M. Popoola, Characteristic Effect of Alloying Elements on β Solidifying Titanium Aluminides: A Review, *Heliyon*, 2020, **6**(7), p e04463. <https://doi.org/10.1016/j.heliyon.2020.e04463>
3. B.P. Bewlay, S. Nag, A. Suzuki, and M.J. Weimer, TiAl alloys in Commercial Aircraft Engines, *Mater. High Temp.*, 2016, **33**(4-5), p 549-559. <https://doi.org/10.1080/09603409.2016.1183068>
4. H. Clemens and S. Mayer, Intermetallic Titanium Aluminides in Aerospace Applications – Processing, Microstructure and Properties, *Mater. High Temp.*, 2016, **33**(4-5), p 560-570. <https://doi.org/10.1080/09603409.2016.1163792>
5. B.P. Bewlay, M. Weimer, T. Kelly, A. Suzuki, and P.R. Subramanian, The Science, Technology, and Implementation of TiAl Alloys in Commercial Aircraft Engines, *MRS Online Proc. Library (OPL)*, 2013, **1516**, p 49-58. <https://doi.org/10.1557/opl.2013.44>
6. L. Song, X.J. Xu, L. You, Y.F. Liang, and J.P. Lin, Phase Transformation and Decomposition Mechanisms of the $\beta_0(\omega)$ Phase in Cast High Nb Containing TiAl Alloy, *J. Alloy. Compd.*, 2014, **616**, p 483-491. <https://doi.org/10.1016/j.jallcom.2014.07.130>
7. K. Das and S. Das, Order-Disorder Transformation of the Body Centered Cubic Phase in the Ti-Al-X (X = Ta, Nb, or Mo) System, *J. Mater. Sci.*, 2003, **38**, p 3995-4002. <https://doi.org/10.1023/A:1026262616194>
8. B. Distl, K. Hauschildt, F. Pyczak, and F. Stein, Solid-Solid Phase Transformations and Their Kinetics in Ti–Al–Nb Alloys, *Metals*, 2021, **11**(12), p 1991. <https://doi.org/10.3390/met11121991>
9. H. Zhang, N. Yan, H. Liang, and Y. Liu, Phase Transformation and Microstructure Control of Ti₂AlNb-Based Alloys: A Review, *J. Mater. Sci. Technol.*, 2021, **80**, p 203-216. <https://doi.org/10.1016/j.jmst.2020.11.022>
10. T.B. Massalski, Binary Alloy Phase Diagrams. 2nd ed, 1990, ASM International, Metals Park, OH, USA, p. 2179-2181.
11. J. Braun and M. Ellner, On the Partial Atomic Volume of Aluminium in the Titanium-Rich Phases of the Binary System Ti-Al, *Z. Met.*, 2000, **91**(5), p 389-392.
12. J. Braun, M. Ellner, and B. Predel, Experimental Investigations of the Structure and Stability of the TiAl Phases (in German), *Z. Met.*, 1995, **86**(12), p 870-876. <https://doi.org/10.1515/ijmr-1995-861212>
13. P.J. Brown and J.B. Forsyth, The Structure of the σ -Phase Nb₂Al, *Acta Crystallogr. A*, 1961, **14**(4), p 362-364. <https://doi.org/10.1107/s0365110x61001248>
14. E.A. Wood, V.B. Compton, B.T. Matthias, and E. Corenzwit, β -Wolfram Structure of Compounds Between Transition Elements and Aluminum, Gallium and Antimony, *Acta Crystallogr. A*, 1958, **11**(9), p 604-606.
15. L.A. Bendersky, W.J. Boettinger, B.P. Burton, F.S. Biancaniello, and C.B. Shoemaker, The Formation of Ordered ω -Related Phases in Alloys of Composition Ti₄Al₃Nb, *Acta Metall. Mater.*, 1990, **38**(6), p 931-943. [https://doi.org/10.1016/0956-7151\(90\)90165-D](https://doi.org/10.1016/0956-7151(90)90165-D)
16. D. Banerjee, A.K. Gogia, T.K. Nandi, and V.A. Joshi, A New Ordered Orthorhombic Phase in a Ti₃Al-Nb Alloy, *Acta Metall.*, 1988, **36**(4), p 871-882. [https://doi.org/10.1016/0001-6160\(88\)90141-1](https://doi.org/10.1016/0001-6160(88)90141-1)
17. A.V. Pavlov, A.M. Zakharov, G.V. Karsanov, and L.L. Vargasova, Isothermal Sections of the Nb-Ti-Al System at 900°C and 600°C, *Russ. Metall.*, 1992, **1992**(5), p 117-119.
18. R.G. Rowe, D. Banerjee, K. Muraleedharan, M. Larsen, E.H. Hall, D.G. Konitzer, and A.P. Woodfield, Phase Equilibria in Ti-Al-Nb Alloys Near Ti₂NbAl, in *Titanium '92 Science and Technology*. F.H. Froes and I. Caplan, Eds., Metals and Materials Society, The Minerals, 1993
19. D.B. Miracle, M.A. Foster, and C.G. Rhodes, Phase equilibria in Ti-Al-Nb orthorhombic alloys, In: *Titanium '95- Science and Technology*, (1996), p 372-379.
20. F.-A. Sadi, Contribution à l'étude du Diagramme de Phases du Système Al–Nb–Ti au Voisinage Des Composés AlNbTi₂ et Al₃NbTi₄, Ph.D. Thesis, Université de Paris-Sud, Paris. (1997) p 244.
21. F.-A. Sadi and C. Servant, In Situ Neutron Diffraction on the Alloy 50.6Ti-36.5Al-12.9 Nb (at.%), *Z. Met.*, 2000, **91**, p 504-509.
22. X. Shuai, J. Lin, Y. Liang, J. He, X. Chen, L. Cha, and X. Jiang, Phase Stabilities and Equilibria of the Ti-Al-Nb Ternary System at Intermediate Temperatures I. the 900 °C Isothermal Section, *J. Alloys Compd.*, 2022, **900**, p 163399. <https://doi.org/10.1016/j.jallcom.2021.163399>
23. F.A. Sadi, C. Servant, and G. Cizeron, Phase Transformations in Ti–29.7Al–21.8Nb and Ti–23.4Al–31.7Nb (at.%) Alloys, *Mater. Sci. Eng. A*, 2001, **311**(1-2), p 185-199. [https://doi.org/10.1016/S0921-5093\(01\)00912-1](https://doi.org/10.1016/S0921-5093(01)00912-1)
24. C. Servant and I. Ansara, Thermodynamic Assessment of the Al-Nb-Ti System, *Ber. Bunsenges. Phys. Chem.*, 1998, **102**(9), p 1189-1205. <https://doi.org/10.1002/bbpc.19981020923>
25. C.J. Boehlert, The Phase Evolution and Microstructural Stability of an Orthorhombic Ti-23Al-27Nb Alloy, *J. Phase Equilibria*, 1999, **20**(2), p 101-108. <https://doi.org/10.1007/s11669-999-0007-z>
26. C.J. Boehlert, B.S. Majumdar, V. Seetharaman, and D.B. Miracle, Part I. The Microstructural Evolution in Ti-Al-Nb O+Bcc Orthorhombic Alloys, *Metallurgical Mater. Trans. A*, 1999, **30**(9), p 2305-2323. <https://doi.org/10.1007/s11661-999-0240-4>
27. Y. Zhao, L.-B. Liu, L.-G. Zhang, J.-J. Yang, and P.J. Masset, The Polythermal Section of Ti-22Al-xNb (30-78at.%Ti) in Ti-Al-Nb System, *Metals*, 2020, **10**(7), p 871. <https://doi.org/10.3390/met10070871>
28. H.T. Kestner-Weykamp, C.H. Ward, T.F. Broderick, and M.J. Kaufman, Microstructures and Phase Relationships in the Ti₃Al + Nb System, *Scr. Metall.*, 1989, **23**, p 1697-1702. [https://doi.org/10.1016/0036-9748\(89\)90345-1](https://doi.org/10.1016/0036-9748(89)90345-1)
29. K. Muraleedharan, A.K. Gogia, T.K. Nandy, D. Banerjee, and S. Lele, Transformations in a Ti-24Al-15Nb Alloy: Part I, *Phase*

- Equilibria Microstruct. Metallurgical Trans. A*, 1992, **23**(2), p 401-415. <https://doi.org/10.1007/BF02801158>
30. L.A. Bendersky, A. Roytburd, and W.J. Boettinger, Phase Transformations in the (Ti, Al)₃Nb Section of the Ti-Al-Nb System—I. Microstructural Predictions Based on a Subgroup Relation Between Phases, *Acta Metall. Mater.*, 1994, **42**(7), p 2323-2335. [https://doi.org/10.1016/0956-7151\(94\)90311-5](https://doi.org/10.1016/0956-7151(94)90311-5)
 31. K. Muraleedharan, T.K. Nandy, D. Banerjee, and S. Lele, Phase Stability and Ordering Behaviour of the O Phase in Ti-Al-Nb Alloys, *Intermetallics*, 1995, **3**(3), p 187-199. [https://doi.org/10.1016/0966-9795\(95\)98930-7](https://doi.org/10.1016/0966-9795(95)98930-7)
 32. L.A. Bendersky, W.J. Boettinger, and A. Roytburd, Coherent Precipitates in the b.c.c./Orthorhombic Two-Phase Field of the Ti-Al-Nb System, *Acta Metall. Mater.*, 1991, **39**(8), p 1959-1969. [https://doi.org/10.1016/0956-7151\(91\)90165-W](https://doi.org/10.1016/0956-7151(91)90165-W)
 33. X. Yong, Y. Liang, L. Song, G. Hao, B. Tian, X. Rongfu, and J. Lin, Experimental Phase Equilibria and Isoleth Section of 8Nb-TiAl Alloys, *Metals*, 2021, **11**(8), p 1229. <https://doi.org/10.3390/met11081229>
 34. U.R. Kattner and W.J. Boettinger, Thermodynamic Calculation of the Ternary Ti-Al-Nb System, *Mater. Sci. Eng., A*, 1992, **152**(1-2), p 9-17. [https://doi.org/10.1016/0921-5093\(92\)90039-4](https://doi.org/10.1016/0921-5093(92)90039-4)
 35. V.T. Witusiewicz, A.A. Bondar, U. Hecht, and T.Y. Velikanova, The Al-B-Nb-Ti System, *J. Alloys Compd.*, 2009, **472**(1-2), p 133-161. <https://doi.org/10.1016/j.jallcom.2008.05.008>
 36. B. Distl, K. Hauschildt, F. Pyczak, and F. Stein, Phase Equilibria in the Ti-Rich Part of the Ti-Al-Nb System Part II. High-Temperature Phase equilibria Between 1000 and 1300 °C in Preparation for Publication in Journal of Phase Equilibria and Diffusion, (2022).
 37. X. Llovet, A. Moy, P.T. Pinard, and J.H. Fournelle, Electron Probe Microanalysis: A Review of Recent Developments and Applications in Materials Science and Engineering, *Prog. Mater. Sci.*, 2021, **116**, p 100673. <https://doi.org/10.1016/j.pmatsci.2020.100673>
 38. A.A. Kodentsov, G.F. Bastin, and F.J.J. van Loo, The Diffusion Couple Technique in Phase Diagram Determination, *J. Alloy. Compd.*, 2001, **320**(2), p 207-217. [https://doi.org/10.1016/S0925-8388\(00\)01487-0](https://doi.org/10.1016/S0925-8388(00)01487-0)
 39. A.D. Romig, Thermodynamic Considerations in the Analysis of Phase Stability: The Role of Interfacial Equilibrium in the Determination of Phase Diagrams by X-ray Microanalytical Techniques, *Bull. Alloy Phase Diagr.*, 1987, **8**(4), p 308-322. <https://doi.org/10.1007/BF02869262>
 40. N. Schell, A. King, F. Beckmann, T. Fischer, M. Müller, and A. Schreyer, The High Energy Materials Science Beamline (HEMS) at PETRA III, *Mater. Sci. Forum*, 2014, **772**, p 57-61. <https://doi.org/10.4028/www.scientific.net/MSF.772.57>
 41. A. Hammersley, FIT2D: a Multi-Purpose Data Reduction, Analysis and Visualization Program, *J. Appl. Crystallogr.*, 2016, **49**(2), p 646-652. <https://doi.org/10.1107/S1600576716000455>
 42. L. Lutterotti, Total Pattern Fitting for the Combined Size-Strain-Stress-Texture Determination in Thin Film Diffraction, *Nucl. Instrum. Methods Phys. Res., Sect. B*, 2010, **268**(3), p 334-340. <https://doi.org/10.1016/j.nimb.2009.09.053>
 43. G. Yang, X. Yang, Y. Wang, L. Cheng, H. Kou, Y. Liu, Y. Li, P. Wang, and W. Ren, Phase Precipitation Behavior of a Quenched β -Solidifying TiAl Alloy with a Fully-B2 Microstructure During Annealing at 800°C, *J. Alloy. Compd.*, 2020, **812**, p 152118. <https://doi.org/10.1016/j.jallcom.2019.152118>
 44. J.C. Schuster and M. Palm, Reassessment of the Binary Aluminium-Titanium Phase Diagram, *J. Phase Equilib. Diffus.*, 2006, **27**(3), p 255-277. <https://doi.org/10.1361/154770306X109809>
 45. M. Palm, Al-Ti Binary Phase Diagram Evaluation, in MSI Eureka, Effenberg, G. (Ed.) by MSI, Materials Science International Services GmbH, Stuttgart, Doc-ID: 20.15634.2.4., (2020)
 46. H. Okamoto, Nb-Ti (Niobium-Titanium), *J. Phase Equilibria*, 2002, **23**(6), p 553-553. <https://doi.org/10.1361/105497102770331325>
 47. H.F. Chladil, H. Clemens, G.A. Zickler, M. Takeyama, E. Kozeschnik, A. Bartels, T. Buslaps, R. Gerling, S. Kremmer, L. Yeoh, and K.-D. Liss, Experimental Studies and Thermodynamic Simulation of Phase Transformations in High Nb Containing γ -TiAl based Alloys, *Int. J. Mater. Res.*, 2007, **98**(11), p 1131-1137. <https://doi.org/10.3139/146.101569>
 48. M.W. Rackel, A. Stark, H. Gabrisch, and F. Pyczak, Screening for O Phase in Advanced γ -TiAl Alloys, *Intermetallics*, 2021, **131**, p 107086. <https://doi.org/10.1016/j.intermet.2021.107086>
 49. C.-R. Dai, Z.-B. Yang, J. Sun, S. Lu, and L. Vitos, Composition and Temperature Dependence of α_2 Phase Decomposition in High Nb-Containing Lamellar γ -TiAl Alloys: Experiments and First-Principles Calculations, *Acta Mater.*, 2021, **221**, p 117419. <https://doi.org/10.1016/j.actamat.2021.117419>
 50. D.G. Konitzer, I.P. Jones, and H.L. Fraser, Site Occupancy in Solid-Solutions of Nb in the Intermetallic Compounds TiAl and Ti₃Al, *Scr. Metall.*, 1986, **20**(2), p 265-268. [https://doi.org/10.1016/0036-9748\(86\)90139-0](https://doi.org/10.1016/0036-9748(86)90139-0)
 51. D. Holec, R.K. Reddy, T. Klein, and H. Clemens, Preferential Site Occupancy of Alloying Elements in TiAl-Based Phases, *J. Appl. Phys.*, 2016, **119**(20), p 205104. <https://doi.org/10.1063/1.4951009>
 52. Z.W. Huang and T. Cong, Microstructural Instability and Embrittlement Behaviour of an Al-lean, High-Nb γ -TiAl-Based Alloy Subjected to a Long-Term Thermal Exposure in Air, *Intermetallics*, 2010, **18**(1), p 161-172. <https://doi.org/10.1016/j.intermet.2009.07.007>
 53. M.W. Rackel, A. Stark, H. Gabrisch, N. Schell, A. Schreyer, and F. Pyczak, Orthorhombic Phase Formation in a Nb-rich γ -TiAl Based Alloy – An in situ Synchrotron Radiation Investigation, *Acta Mater.*, 2016, **121**, p 343-351. <https://doi.org/10.1016/j.actamat.2016.09.030>
 54. T.H. Yu and C.H. Koo, Microstructural Evolution of a Hot-Rolled Ti-40Al-10Nb Alloy, *Mater. Sci. Eng., A*, 1997, **239**-**240**, p 694-701. [https://doi.org/10.1016/S0921-5093\(97\)00654-0](https://doi.org/10.1016/S0921-5093(97)00654-0)
 55. L. Song, X. Xu, L. You, Y. Liang, Y. Wang, and J. Lin, Ordered α_2 to ω_0 Phase Transformations in High Nb-Containing TiAl Alloys, *Acta Mater.*, 2015, **91**, p 330-339. <https://doi.org/10.1016/j.actamat.2015.03.025>
 56. B. Distl, G. Dehm, and F. Stein, Effect of Oxygen on High-Temperature Phase Equilibria in Ternary Ti-Al-Nb Alloys, *Z. Anorg. Allg. Chem.*, 2020, **646**(14), p 1151-1156. <https://doi.org/10.1002/zaac.202000098>
 57. L. Song, J. Lin, T. Zhang, and J. Li, Precipitation Behavior of α_2 Phase in Ti-34Al-13Nb Alloy, *J. Alloy. Compd.*, 2017, **725**, p 155-162. <https://doi.org/10.1016/j.jallcom.2017.07.079>
 58. L.A. Bendersky, W.J. Boettinger, and F.S. Biancianiello, Intermetallic Ti-Al-Nb Alloys Based on Strengthening of the Orthorhombic Phase by ω -Type Phases, *Mater. Sci. Eng., A*, 1992, **152**(1-2), p 41-47. [https://doi.org/10.1016/0921-5093\(92\)90044-2](https://doi.org/10.1016/0921-5093(92)90044-2)
 59. C.B. Shoemaker, D.P. Shoemaker, and L.A. Bendersky, Structure of ω -Ti₃Al_{2.25}Nb_{0.75}, *Acta Crystallogr. C*, 1990, **46**(3), p 374-377. <https://doi.org/10.1107/S0108270189008504>
 60. S.V. Kamat, A.K. Gogia, and D. Banerjee, Effect of Alloying Elements and Heat Treatment on the Fracture Toughness of Ti-Al-Nb Alloys, *Acta Mater.*, 1998, **46**(1), p 239-251. [https://doi.org/10.1016/S1359-6454\(97\)00207-3](https://doi.org/10.1016/S1359-6454(97)00207-3)